No frag

Observations of Lower Hybrid Resonance Phenomena with the Injun 5 Satellite

by

Roger Russell Anderson

A thesis submitted in partial fulfillment of the
requirements for the degree of Master of Science
in the Department of Physics and Astronomy
in the Graduate College of
The University of Iowa

June 1969

Thesis supervisor: Associate Professor Donald A. Gurnett

Graduate College
The University of Iowa
Iowa City, Iowa

CERTIFICATE OF APPROVAL

MASTER'S THESIS

This is to certify that the Master's Thesis of

Roger Russell Anderson

with a major in Physics has been approved by the Examining Committee as satisfactory for the thesis requirement for the Master of Science degree at the convocation of June 6, 1969.

Thesis committee: Donald A. Bennett
Thesis supervisor

L. A. Franks
Member

John Schwartz
Member

ACKNOWLEDGMENTS

I wish to thank Professor Donald Gurnett for suggesting this study, for his helpful advice that kept the study progressing, and for his assistance in interpreting the data and results. I also wish to thank Mr. Bill Pfeiffer and Mr. Dan Odem who along with Professor Gurnett were responsible for the production and success of the Injun 5 VLF experiment.

I am most indebted to Mrs. Dora Walker for her tireless processing of the data and assistance whenever needed in all aspects of VLF data reduction. I wish to thank Mr. Don Forbes for his overall assistance in this study from processing data and measuring cutoff frequencies to interpolating orbit parameters and especially for his photographic work. I also thank Miss Sheri Hogue for her secretarial assistance and for helping interpolate the orbit parameters.

I also thank Mr. Harry Melander for the magnetometer plot programs, Mr. Robert Brechwald for supplying time and orbit parameters, and Miss Ruth Rogers and her assistants for key-punching orbit cards.

A special thanks go to the drafting department and especially Mrs. Sala Knipfer, Mrs. Janet Wilkinson, and Mr. John Birkbeck for

their excellent work and patience under pressure. I also thank Mrs. Pamela Kostel for her careful typing of this paper.

This work was supported in part by the National Aeronautics and Space Administration under contracts NAS1-8141, NAS5-10625, NAS1-8144(f), NAS1-8150(f), and NGR-16-001-043 and by the Office of Naval Research under contract Nonr 1509(06).

ABSTRACT

A study of lower hybrid resonance (LHR) phenomena observed by the VLF experiment on the Injun 5 satellite is presented. The occurrence and characteristics of the mid-latitude and polar LHR noise bands are similar to past observations on other satellites. Several new LHR phenomena are identified, including reflection phenomena, multiple noise bands, and spin-modulated LHR bands. In agreement with cold-plasma theory and typical ionospheric models, some whistlers propagating transverse to the magnetic field have reflected components beginning just below the local LHR frequency up to an upper cutoff which is identified as the maximum LHR frequency with altitude. Multiple noise bands associated with the local LHR frequency but not equal to it are observed several times in conjunction with the LHR noise band. Some of the multiple bands are electromagnetic and some appear to be associated with the upper frequency cutoff observed for reflection phenomena. Spin-modulated LHR noise bands are observed very frequently. The lower cutoff frequency of the LHR noise band is modulated at the spin rate of the satellite. The modulation characteristics are related to the asymmetric shape of the satellite and booms. Probable cause for the modulation is either the doppler effect or generation of the noise by the spacecraft moving through the plasma.

TABLE OF CONTENTS

LIST OF FIGURES

LIST OF FIGURES (cont'd.)

I. INTRODUCTION

It is the purpose of this paper to discuss lower hybrid resonance (LHR) phenomena and to present a study of LHR phenomena observed by the very low frequency (VLF) experiment on the Injun 5 satellite. This study includes a description of LHR phenomena, including that seen previously and several types observed or identified for the first time in Injun 5 data, spatial and spectral profiles of the various observed phenomena, and possible explanations for the observed phenomena.

LHR phenomena were first observed on the Alouette 1 satellite by Barrington and others [Barrington et al., 1963; Barrington and Belrose, 1963; Belrose and Barrington, 1965] as noise bands in the 5-10 kHz range having a sharp lower-frequency cutoff. The Alouette 1 observations were made using a broadband VLF receiver connected to a 150-foot electric dipole. Alouette 1 was in a nearly polar and nearly circular orbit with an altitude of 1000 km. From comparisons of satellite and ground station observations, Brice and Smith [1964] found that these noise bands were not seen on the ground.

Brice and Smith [1964, 1965] also concluded that the lower-frequency cutoff of the noise bands was the LHR frequency (f_{LHR})

of the ambient plasma. This conclusion was based on the following facts. The only resonance for frequencies in the range of interest is the f_{LHR}. This frequency defines a cutoff frequency for propagation transverse to the static magnetic field. For wave normal angles less than 90° the frequency of resonance is higher than the f_{LHR}. Thus the frequencies at which resonance can occur have a natural lower-frequency cutoff. Triggering of LHR noise bands is more likely for non-ducted whistlers which indicates propagation at large wave normal angles. For frequencies near f_{LHR} the dominant wave field component is the wave electric field in the wave normal direction. In agreement with this, LHR noise was much more common on Alouette 1 with an electric dipole antenna than on Injun 3 having a magnetic loop antenna. Brice and Smith also found that the effective mass required for the observed bands to have the f_{LHR} as the lower-frequency cutoff is not unreasonable. The theoretical basis for these properties will be discussed in Section II.

McEwen and Barrington [1967] in a study of the characteristics and occurrences of LHR phenomena observed by Alouette 1 identified two types of LHR noise--mid-latitude and polar LHR noise. The mid-latitude type has a fairly sharp lower-frequency cutoff, which is nearly constant or only slowly varying in time,

and varies in duration from short bursts directly triggered by whistlers to more continuous emissions. The polar type has an erratic and fluctuating lower cutoff frequency and no observable triggering. The polar type was found to be concentrated in regions from 70° to 85° invariant latitude (INV) while the mid-latitude type occurred primarily between 45° and 60° INV. The region near 65° INV was noted to have little LHR activity. The mid-latitude noise bands occurred mainly during the months from May to October while the polar noise bands occurred throughout the year. The mid-latitude type occurred primarily at night with a peak slightly before midnight and a secondary peak about 0600-0800 hours local time (LT). The polar bands were present much of every day but also had two maxima at the same time as the mid-latitude type.

Prior to this paper, the most recent observations of LHR phenomena have been done by Laaspere et al. [1969] using data from Dartmouth's whistler receiver which was connected to a 9-foot electric dipole antenna aboard the OGO 2 spacecraft. Even though their antenna was much shorter than Alouette's, Laaspere et al. found similar results to the Alouette observations. LHR noise bands were the second most intense VLF signals observed, next only to short fractional-hop whistlers. From a direct comparison made of records obtained simultaneously on OGO 2 by Stanford's

VLF experiment which is connected to a loop antenna, it is shown that triggered LHR emissions are seen almost exclusively on Dartmouth's experiment, pointing to an electric character for the waves. A new observation made by the Dartmouth experiment is that the upper cutoff frequency of the LHR noise bands triggered by fractional-hop whistlers occasionally displays an envelope that has the shape of an Eckersley whistler.

Many origins of the observed LHR phenomena have been suggested. Brice et al. [1964] concluded that since the triggering by atmospherics which are propagating up the field indicates that the noise is generated at or below the satellite and the triggering by whistlers believed to be propagating down the field suggests generation at or above the satellite, the LHR noise must be generated at the same height as the satellite. Since the sharp lower frequency cutoff of the noise changes measurably in a few seconds, Brice and Smith [1964] concluded that the horizontal field of view for the LHR noise bands is at most a few tens of kilometers and thus noise must be generated in the immediate vicinity of the satellite. They suggest the LHR noise band arises from a resonance in the plasma for very low frequencies.

Brice and Smith [1965] offer a simple physical model for the LHR resonance. At night when LHR is most frequently observed

and at the Alouette 1 altitude, the electron plasma frequency is usually less than the electron gyrofrequency for latitudes of interest. In this situation the f_{LHR} is approximately the ion plasma frequency. As the resonance frequency is much less than the electron gyrofrequency, the electrons can be considered as tightly bound by the earth's magnetic field. Since the ion gyrofrequency is much less than the resonance frequency, the ions are considerably more mobile. Thus if the ions are displaced across the static magnetic field, the tightly bound electrons form a fixed negatively charged background and the ions oscillate at their plasma frequency in a manner similar to electrons in the absence of a magnetic field.

Smith et al. [1966] suggest that the LHR noise is essentially a propagation effect resulting from the trapping of electromagnetic waves propagating nearly transverse to the magnetic field in an ionospheric duct or cavity. Using a typical ionospheric model from Kimura [1966] they calculated the variation of f_{LHR} with altitude as shown in Figure 1. The lower maximum results from the maximum of plasma frequency in the F layer. The increase with altitude at about 500 km is mainly due to the rapid decrease in effective mass in the transition from oxygen to hydrogen ions. The final decrease with altitude above 1000 km results from a decrease of both plasma frequency and gyrofrequency with altitude.

Smith et al. [1966] calculated the variation of refractive index with height for a wave of frequency 5.25 kHz with a wave normal transverse to the earth's magnetic field. Their results are also shown in Figure 1. They assumed the magnetic field was vertical and that stratification was horizontal. They found from Snell's law which requires that the component of refractive index in the plane of stratification be constant that a nearly transverse wave with a horizontal component of refractive index greater than 700 would be trapped in region II between 500 and 785 km. For a satellite at a fixed altitude the approximate frequency range of trapped energy that would be observed is from slightly below the local f_{LHR} up to the lower of the two maximums of f_{LHR} with altitude. Thus this hypothesis leads to an explanation of both the upper and lower frequency limits of LHR noise. To observe the LHR trapping a f_{LHR} minimum with altitude must exist and the satellite must be in the proper height range between the two f_{LHR} maximums. Smith et al. felt that a variation of temperature and ion constituents with latitude and season could be expected to produce changes in occurrence rates and observable bandwidths of LHR noise.

Ray tracing calculations have verified the possibility of the above trapping and have found two more trapping regions, III

and IV, shown in Figure 1. However, of the three, region II has the least attenuation. The calculations show that the rays are confined principally to travel back and forth along magnetic field lines with very little transverse motion. Thus the trapping region resembles a cavity resonator.

To explain the excitation of the mode, Smith et al. [1966] suggested that nearly longitudinal waves above the f_{LHR} can be partially converted to nearly transverse waves upon encountering field-aligned irregularities. Experimental support for this suggestion is shown by the LHR whistler which exhibits added dispersion near the LHR frequency, strongly suggesting nearly transverse propagation.

McEwen and Barrington [1967] in a preliminary study of Alouette 2 VLF data have observed LHR noise bands over the full range of heights of the orbit, from 500 km to 3000 km. They feel it is not possible to reconcile these observations with the trapped whistler energy source suggested by Smith et al. [1966] because this mechanism would permit generation of LHR noise bands over a well-defined height region only.

Ray tracing calculations by Kimura [1966] and Shawhan [1967] have shown that ray paths for frequencies below 12 kHz reflect before reaching the base of the ionosphere and are essentially

trapped in the magnetosphere. The altitude of the reflection is approximately the altitude for which the f_{LHR} is equal to the wave frequency.

McEwen and Barrington [1967] noted that the diurnal maxima for LHR observations are similar to those of other auroral-zone geophysical phenomena and therefore suggest a possible relation between polar LHR noise bands, auroral activity, and particle precipitation. In many cases the mid-latitude LHR bands appear to be generated or triggered by whistlers. This is supported by the study of Laaspere et al. [1963] that noted that whistlers recorded on the ground and the mid-latitude LHR noise bands have the same general pattern of occurrence. McEwen and Barrington [1967] suggest that the whistler mode energy radiated from lightning discharges may be the sole source of the mid-latitude noise bands. They also suggest that the observed rapid fluctuations of the lower-frequency cutoff are most probably due to irregularities in electron density of the plasma surrounding the spacecraft.

Another possible origin for the VLF noise being considered is the generation by trapped electrons of whistler mode waves in equatorial high L regions. Thorne and Kennel [1967] studied the propagation of whistler noise so generated. They found that the wave normal direction for waves originating at the equator rapidly becomes almost perpendicular to the magnetic field. Considering

propagation near the f_{LHR} they found that low-frequency waves will be reflected before reaching the ionosphere and thus be quasi-trapped. The waves tend to move to higher L values as they approach the earth and would on reflection move out farther. Thus on each reflection the waves move out to a slightly higher L shell. This migration outward on several reflections is in general agreement with the detailed ray tracing calculations of Kimura [1966] and Shawhan [1967].

Storey and Cerisier [1968] have enlarged upon the work of Thorne and Kennel [1967] with respect to frequencies near the f_{LHR} in order to interpret the LHR noise bands. They follow Thorne and Kennel's suggestion that VLF noise in the whistler mode is generated in the outer magnetosphere as the result of a plasma instability induced by the energetic electrons of the outer radiation belt. The source region is centered on the magnetic equatorial plane from where the waves are propagated towards the ground in the two hemispheres nearly following the magnetic field lines. During the propagation the wave normals turn away from the direction of the field under the combined influences of the gradient of the magnetic field strength and the curvature of the field lines, and place themselves on the flanks of the refractive index surface, almost perpendicular to the field lines. The

angle θ between the wave-normal and the magnetic field increases to almost 90°. The downcoming wave packet traverses a medium in which the f_{LHR} increases with decreasing altitude. As soon as the packet reaches the level at which the f_{LHR} exceeds the wave frequency, θ passes through 90° and the packet is reflected back upwards. As the wave-normal (propagation) vector cannot pass through the resonance angle it cannot pass through 90° until the wave frequency is below the f_{LHR}. Below the f_{LHR} the refractive index surface does not display a resonance angle and thus the wave normal can pass through 90° and the wave can be reflected. Figure 2 shows an exaggerated view of the path of a typical wave packet. Figure 3 shows the axial cross-section of the phase refractive index surface for the three cases $f > f_{LHR}$, $f = f_{LHR}$, and $f < f_{LHR}$. The location on the phase refractive index surface of the five points marked in Figure 2 is also shown in addition to the wave-normal direction and the direction of energy propagation (or ray direction) which is perpendicular to the refractive index surface. As the wave frequency moves below the f_{LHR} the index of refraction surface shrinks. Snell's law requires the perpendicular component of the index of refraction to be constant. Thus θ must move toward 90° and the wave will be reflected.

It was the purpose of Storey and Cerisier to show that the VLF noise produced by the mechanism described by Thorne and Kennel should exhibit at the altitude of reflection a power spectrum similar to that of the noise bands observed by the satellite. To do this they made two additional hypotheses: first that the original noise is wideband, as could be expected from the instability theory, and the second that the source region is large. The second hypothesis is needed to ensure that at the low reflection altitudes waves of all frequencies will arrive together around the line of force that passes through the center of the source region even though they have followed different paths.

Storey and Cerisier assumed that at the level of the satellite f_{LHR} decreases with increasing altitude and that it does not recover the same value at any higher level. f_o is identified as the frequency of a wave that is just reflected at the level of the satellite. From the reflection process one knows f_o is only very slightly lower than f_{LHR}. Let f_+ be slightly above f_{LHR} and f_- be slightly below f_o. It was assumed these frequencies have all been generated with approximately the same original intensities.

In considering its contribution to the spectrum of the observed noise, the wave of frequency f_o is very strong for two reasons. Ignoring absorption, the conservation of vertical energy flux implies that the average intensity of a wave packet in a given interval of altitude is proportional to the time that the packet spends in that interval. In the narrow interval that includes the reflection level where the vertical velocity passes through zero and changes direction, the time spent by the packet is much longer than the time spent on the same thickness interval at any other altitude. This causes the intensity of the f_o wave packet to be much greater than any other frequencies at the reflected altitude. An additional enhancement occurs for noise observed using an electric dipole antenna. Near f_{LHR} the polarization of the waves is such that the component of the electric field along the wave normal is particularly strong for a given energy flux. For these two reasons the power spectrum of the noise bands attains a maximum near f_{LHR}.

The wave of frequency f_- does not appear in the spectrum because it has been reflected at a level above that of the satellite. This same consideration applies to all frequencies below f_o and explains why the spectrum has a sharp cutoff at its low-frequency edge.

The wave of frequency f_+ appears in the spectrum because it has crossed the level of the satellite both before and after being reflected at some level below the satellite. Its contribution to the spectrum is less than that for the wave of frequency f_o because it has spent less time around the level of the satellite and because the longitudinal component of its electric field is weaker in proportion to the energy flux. The more f_+ exceeds f_o, the less it will contribute to the spectrum. These considerations explain why the noise band is fairly narrow and why there is no sharp upper-cutoff frequency.

Taking into account that there will be a finite spread of the wave-normal directions, one sees that the waves will be reflected in an altitude interval of finite thickness. Any wave normal angle less than 90° will be reflected at a higher altitude. This spread in wave normal angles rounds off the spectrum of the observed noise. Figure 4 shows the results of a calculation by Storey and Cerisier of the intensity spectrum of the noise band in a typical case, at a point where the local f_{LHR} is equal to 8.5 kHz and f_{LHR} decreases monotonically with altitude.

II. PROPERTIES OF LHR FROM COLD PLASMA THEORY

One form of the dispersion relation for waves in cold uniform plasmas with a magnetic field is given by Stix [1962, p. 12] as

$$\tan^2\theta = \frac{-P(n^2 - R)(n^2 - L)}{(Sn^2 - RL)(n^2 - P)}$$

where θ = the angle between the wave normal and the static magnetic field

n = the phase refractive index

$P = 1 - \sum_s \omega_{p_s}^2/\omega^2$

$R = 1 - \sum_s \omega_{p_s}^2/\omega(\omega + \omega_{g_s})$

$L = 1 - \sum_s \omega_{p_s}^2/\omega(\omega - \omega_{g_s})$

$S = \frac{1}{2}(R + L)$

$\omega_{p_s}^2 = N_s e_s^2/\epsilon_o m_s$ is the square of the plasma frequency of the s^{th} constituent

$\omega_{g_s} = e_s B/m_s$ is the gyrofrequency of the s^{th} constituent

B = static magnetic field strength

ω = wave frequency in radians per second.

For propagation perpendicular to the magnetic field ($\theta = 90°$), solutions to the dispersion relation are either $n^2 = RL/S$ or $n^2 = P$. The $n^2 = P$ mode is called the ordinary mode and corresponds to a linearly polarized electromagnetic wave propagating perpendicular to $\vec{B}$. The $n^2 = RL/S$ mode has an electric field with both longitudinal and transverse parts. The $n^2 = RL/S$ mode is called the extraordinary mode. As the wave frequency approaches the resonance frequencies for this mode (where $S = 0$) the longitudinal electric field becomes much larger than the transverse electric field and the wave becomes electrostatic in nature. The $S = 0$ resonant frequencies are called the hybrid resonances. Resonance occurs when n^2 becomes infinite.

$S = 0$ leads to

$$S = 1 - \tfrac{1}{2}\sum_s \frac{\omega_{p_s}^2}{\omega_r(\omega_r - \omega_{g_s})} - \tfrac{1}{2}\sum_s \frac{\omega_{p_s}^2}{\omega_r(\omega_r + \omega_{g_s})}$$

$$= 1 - \sum_s \frac{\omega_{p_s}^2}{\omega_r^2 - \omega_{g_s}^2} = 0 \quad \text{or} \quad \sum_s \frac{\omega_{p_s}^2}{\omega_r^2 - \omega_{g_s}^2} = 1 .$$

If the ions are singly charged and positive and the plasma is electrically neutral, the preceding equation takes the form

$$\frac{\omega_{p_e}^2}{\omega_r^2 - \omega_{g_e}^2} + \sum_i \frac{\omega_{p_i}^2}{\omega_r^2 - \omega_{g_i}^2} = 1 .$$

Dividing both sides of the equation by $\omega_{p_e}^2/\omega_r^2$ we have

$$\frac{1}{1 - \omega_{g_e}^2/\omega_r^2} + \sum_i \frac{N_i/N_e \; m_e/m_i}{1 - \omega_{g_i}^2/\omega_r^2} = \frac{\omega_r^2}{\omega_{p_e}^2} .$$

Letting $\alpha_i = N_i/N_e$ be the fractional concentration of the i^{th} species, M_i the atomic mass number of the i^{th} species, and m_p the mass of a proton we have

$$\frac{1}{1 - \omega_{g_e}^2/\omega_r^2} + \sum_i \frac{\alpha_i \; m_e/m_p \; 1/M_i}{1 - \omega_{g_i}^2/\omega_r^2} = \frac{\omega_r^2}{\omega_{p_e}^2} .$$

Under most ionospheric conditions the wave frequency at which this resonance occurs is such that $\omega_{g_i}^2/\omega_r^2 \ll 1 \ll \omega_{g_e}^2/\omega_r^2$. With this condition the equation becomes

$$\frac{-\omega_r^2}{\omega_{g_e}^2} + \frac{m_e}{m_p} \sum_i \frac{\alpha_i}{M_i} = \frac{\omega_r^2}{\omega_{p_e}^2} \qquad \text{or}$$

$$\omega_r^2 \left[\frac{1}{\omega_{p_e}^2} + \frac{1}{\omega_{g_e}^2} \right] = \frac{m_e}{m_p} \sum_i \frac{\alpha_i}{M_i} \; .$$

Thus $$\omega_r^2 = \frac{\omega_{p_e}^2 \, \omega_{g_e}^2}{\omega_{p_e}^2 + \omega_{g_e}^2} \frac{m_e}{m_p} \sum_i \frac{\alpha_i}{M_i} \qquad \text{or}$$

$$f_{LHR}^2 = \frac{f_{p_e}^2 \, f_{g_e}^2}{f_{p_e}^2 + f_{g_e}^2} \frac{m_e}{m_p} \sum_i \frac{\alpha_i}{M_i}$$

where f_{LHR} = LHR frequency in Hz

f_{p_e} = electron plasma frequency

$= 8.984 \times 10^3 \, (Ne)^{\frac{1}{2}}$ Hz where Ne is in cm^{-3}

f_{g_e} = electron gyrofrequency

$= 2.8 \times 10^6$ B Hz where B is in gauss.

Following Barrington et al. [1965] we define the "effective mean ion mass number" M_{eff} by

$$\sum_i \frac{\alpha_i}{M_i} = \frac{1}{M_{eff}} .$$

Thus the equation reduces to

$$f_{LHR}^2 = \frac{1}{1836\, M_{eff}} \frac{f_{p_e}^2 f_{g_e}^2}{f_{p_e}^2 + f_{g_e}^2} .$$

A plot of $n^2 = RL/S$ versus frequency for an electron and three ion plasma is shown in Figure 5. The phase velocity surface for frequencies near f_{LHR} as determined by Smith and Brice [1964] are also shown. The corresponding index of refraction surfaces from Storey and Cerisier have been shown previously in Figure 3.

III. DESCRIPTION OF THE SATELLITE AND EXPERIMENT

The NASA/University of Iowa Injun 5 satellite was launched from the Western Test Range on 8 August 1968 into an elliptical polar orbit with an inclination of 80.66°, an apogee altitude of 2528 km, a perigee altitude of 677 km, and a period of revolution of 1 hour 58 minutes. The spacecraft is magnetically oriented by a bar magnet within the structure such that, when properly aligned, the x-axis of the spacecraft is parallel to the geomagnetic field with the positive x-axis downward in the northern hemisphere. The line of separation between the spheres of the electric dipole antenna is parallel to the spacecraft y-axis. The satellite z-axis is also the launch spin-axis and the axis of the balloon cannister. A three-dimensional drawing of the spacecraft including coordinate axes is shown in Figure 6. When the spacecraft is magnetically aligned, the electric antenna axis and the magnetic loop antenna axis are perpendicular to the geomagnetic field as well as to each other.

Shortly after launch the satellite spin rate was approximately 3 rpm. After 1000 revolutions it had slowed to 1 rpm, and by 2000 revolutions the satellite had stopped spinning and was oscillating only slightly with a period of about 8 minutes.

Magnetic alignment was achieved about 4 months after launch in mid-December 1968. Typical maximum alignment errors between the x-axis and the geomagnetic field after mid-December are about 10 to 15 degrees.

The VLF experiment consists of one electric dipole antenna, one magnetic loop antenna, two wide-band (30 Hz to 10 kHz) receivers, a narrow-band step-frequency receiver, an impedance measurement device for determining the electric antenna impedance, and a sphere potential measurement circuit. A block diagram of the VLF experiment is shown in Figure 7.

The electric dipole antenna is of the type described by Storey [1965] and consists of two spherical aluminum antenna elements 20.3 cm in diameter with a center-to-center separation of 2.85 meters. The aluminum booms supporting these antenna elements are insulated from the spheres and from the spacecraft body and are coated with a nonconducting paint to insulate the booms from the surrounding plasma. The electric antenna preamplifiers are high input impedance unity gain amplifiers and are located inside the spheres. These preamplifiers have a noise level of about 10^{-14} volts Hz^{-1}. The unity gain preamplifiers provide signals via coaxial cables inside the booms to a differential amplifier in the main electronics package. The preamplifiers also drive

the aluminum booms supporting the spheres to reduce the sphere-boom capacity. The output of the differential amplifier is proportional to the potential difference, and thus the electric field, between the two spheres. The AC signals from the electric antenna differential amplifier go to a step-frequency receiver and to a wide-band receiver.

The wide-band electric receiver consists of two bandpass filters, each followed by a nonlinear compressor amplifier. These bandpass filters provide a "low"-frequency band of 30 Hz to 650 Hz and a "high"-frequency band of 300 Hz to 10 kHz, which are independent of each other. The nonlinear compressor amplifiers compress the dynamic range of the broad-band analog AC signals from the antenna (80 dB) to a dynamic range (20 dB) suitable for direct transmission to the ground with the 400 MHz telemetry transmitter. The wide-band receiver also provides voltages proportional to the signal amplitude in each band over an 80 dB dynamic range and with a time constant of 0.25 seconds. These amplitude voltages are transmitted via the digital telemetry at a rate of one sample per second. The sensitivities of the high and low band amplitude measurements are both about 10 μvolts rms potential difference between the spheres.

The magnetic loop antenna, whose axis is parallel to the z-axis of the spacecraft, consists of six turns of No. 14 copper wire wound on a circular form 0.56 meters in diameter. The loop wires are electrostatically shielded to prevent the detection of ambient electrostatic waves. The loop antenna is located on the end of a 3-meter boom to reduce electromagnetic interference generated by the spacecraft to an acceptable level.

The magnetic loop antenna is matched to the magnetic pre-amplifier by a transformer with a 1:200 turns ratio. The voltage from the magnetic loop, which is proportional to the time-rate of change of the magnetic field, is integrated to provide a signal proportional to the AC magnetic field. The magnetic field signal goes to a wide-band receiver identical in characteristics to the electric wide-band receiver. The sensitivities of the magnetic high and low bands are approximately 0.5 and 3.0 mγ, respectively.

All four wide-band analog channels are transmitted simultaneously with a single 0.8 watt, 400 MHz telemetry transmitter.

Approximately three hours of wide-band VLF data have been obtained daily from the VLF experiment since launch. The operation of all parts of the VLF experiment mentioned above have been entirely satisfactory.

A more detailed discussion of the Injun 5 VLF experiment can be found in Gurnett et al. [1969].

Gurnett et al. [1969] have shown that the antennas are operating correctly and as expected. The dominant impedance observed by the electric antenna has been the sheath impedance. The observations have shown only small deviations from the resistor-capacitor sheath model and the impedances observed are in reasonably good quantitative agreement with expected values. Observed excursions in the DC sphere potential difference measurements equal to the $\vec{V} \times \vec{B}$ potential due to the satellite motion through the magnetic field show that the effective length for DC electric field measurements is very close to the separation distance between the spheres. By comparing the electric and magnetic field amplitudes for known orientation of the satellite and for known electron number density, it has been shown that the separation distance between the spheres is approximately the effective length of the antenna for AC fields also.

Preflight measurements showed that the electrical coupling between the electric and magnetic receivers is less than -60 dB on a free space basis. Inflight observations have verified that the coupling between the two receivers is negligible. The impedance sweeps which occur on the electric antenna only are

seen infrequently and then only faintly in the magnetic receiver data. The near field of the magnetic interference from the spacecraft which can occur as a fairly strong signal on the magnetic receiver is infrequently seen on the electric receiver and then only faintly. This is because the balanced dipole antenna has a common mode rejection of about -50 dB which strongly attenuates interference signals.

IV. STUDY OF OBSERVED VLF PHENOMENA

The original purpose of this study was to examine LHR phenomena observed by the Injun 5 VLF experiment and to determine LHR occurrence and frequency profiles. An unexpected by-product was the discovery or identification of several new LHR phenomena.

The sample we used consisted primarily of all Injun 5 passes over the University of Iowa NLRO data acquisition facility that occurred ± 3 hours of local midnight and for which VLF analog data were received. A few passes in the sample came from other stations and up to ± 5 hours of local midnight and data from them have been so identified. At the beginning of the study the NLRO tapes were the only readily available data we could use. As data from other stations became available, it was used as needed and as time permitted, especially for data from altitude sectors for which data from NLRO was lacking or unproductive. The time period ± 3 hours of local midnight was chosen to give us a period when the ionosphere was stable thermally. Fortunately the hours we chose also correspond to the hours of maximum rate of occurrence of VLF noise as determined by previous experiments. NLRO was also a fortunate choice for it is a mid-latitude location (~ 41° N geographic latitude) and LHR phenomena having a sharp lower-frequency cutoff are of the mid-latitude type.

The data processing method is described below. The analog tapes from the tracking station were played on a tape recorder and the recorded output from the 400 MHz transmitter was fed into the VLF demodulator. The VLF demodulator separated the four channels of VLF analog data, electric high and low bands and magnetic high and low bands. The band of interest, which in our case was primarily the electric high band, was fed into a spectrum analyzer. At one-minute intervals, time and frequency calibration markers of two-seconds duration were also fed into the spectrum analyzer. On the 0-10 kHz range the spectrum analyzer had a time constant of 0.025 seconds and a frequency resolution of 20 Hz width. An output voltage proportional to the logarithm of the intensity of the frequency being analyzed at a given instant was used to intensity modulate an oscilloscope beam. The more intense the signal, the brighter the beam. A sawtooth voltage from the spectrum analyzer controlled the vertical deflection of the oscilloscope beam. This sawtooth was synchronized to the logarithmic output so that the vertical height on the scope corresponded linearly to the frequency being sampled. The full frequency range was sampled 40 times a second. The spectrum analyzer was so constructed that the gain from each frequency interval being sampled is the same for equal inputs at each frequency. In

other words, the response of the spectrum analyzer was flat from approximately 20 Hz up through 10 kHz.

The oscilloscope screen was photographed using a 35 mm continuous motion instrument camera. The vertical trace on the oscilloscope screen was not swept horizontally in time. The time axis was provided by the continuously moving film. The 100-foot rolls of film were developed and returned to us for analysis. On the film a dark spot corresponds to an intense signal at a given frequency at a given instant in time. A lighter spot corresponds to a less intense signal. The data is continuous and linear both in frequency (from approximately 0 to 10 kHz) and in time. Calibration marks every 1 kHz from 0 kHz to 10 kHz are provided for two seconds every minute on the minute. The time scale on the films should be accurate to less than one second. The films were then visually analyzed to obtain the data used in this study.

The film was projected onto the ground glass screen of an optical-to-digital readout system and the lower-frequency cutoff of the noise bands was measured. The accuracy of the measuring apparatus was ± 10 Hz. However, the accuracy of the frequency measurements is not as small due to the cutoff not being perfectly sharp and also due to a width or spread in the intensity due to the bandwidth of each frequency sample on the spectrum analyzer

not being infinitesimal and also due to the dot size on the oscilloscope not being infinitesimal. A best estimate for the overall minimum error for the measured LHR cutoff frequency is ± 40 Hz.

During the study analog VLF data from 191 revolutions were examined. Eighteen of the revolutions contained no recognizable LHR noise bands or other LHR phenomena. Thirty-nine of the revolutions contained LHR noise bands having a lower-cutoff frequency which could not be measured either because the bands were fluctuating so much the measurements would be meaningless or because interference was present to the extent that the lower-cutoff frequency could not be identified. One hundred thirty-four revolutions contained LHR noise bands with a lower-cutoff frequency that could be measured, of which data from 101 revolutions were measured. The remainder will be measured as equipment and time permit. For the 101 revolutions, the LHR lower-cutoff frequency was measured every five seconds on the data and recorded. For each of these data points the coordinates of the satellite position in space were calculated using the coefficients determined by Jensen and Cain [1962]. The data were then sorted as a function of invariant latitude (INV). Figure 8 is a histogram of measured LHR occurrence as a function of INV. Data for which the LHR cutoff frequency could be measured never occurred below

36° INV nor above 69°. The occurrence of this mid-latitude LHR peaked at 55° INV. These above figures for the Injun 5 VLF experiment agree very well with the observations for Alouette 1 by McEwen and Barrington [1967] noted before. Figure 9 is a graph of occurrence for measured LHR as functions of INV and altitude. The occurrences are most frequent for 45° INV to 60° INV but do not vary greatly in altitude. Our findings agree well with the Alouette 2 observations of McEwen and Barrington [1967] that LHR mid-latitude noise is found at all altitudes from 500 km to 3000 km. On all of the magnetic receiver data from Injun 5 that we have examined we have found no noise bands that have a sharp lower-frequency cutoff which appears to be the LHR cutoff frequency.

We attempted to produce profiles of the LHR cutoff frequency as a function of altitude. Figure 10 shows a typical result. It is for measured LHR bands occurring ± 3 hours of local midnight at the peak location 55° INV. Little can be understood from the graph because of the large amount of scatter in the points. Possibly the only significant information might come from a curve through the maximum LHR cutoff frequency for a given altitude. A curve through such points would appear to be continuous and smoothly varying. A possible explanation for the large scatter

observed is that the ionosphere is slowly changing on a very long time scale. We observe that consecutive passes produce nearly equal LHR cutoff frequencies for the same point in the ionosphere. However, the scatter may be due to widely different LHR cutoff frequencies being observed many days or weeks apart.

The first new LHR phenomena observed on Injun 5 are the reflection phenomena indicated in Figure 11. This figure is a continuous nine-minute frequency-time spectrogram of the electric receiver high-band data from revolution 1173. The frequency scale is from 0 to 10 kHz. From 0621:00 to nearly 0624:00 we observe many long-hop whistlers that become very disperse at the LHR cutoff frequency. The six spectrograms at the bottom are enlarged sections of the upper spectrograms. At approximately 0623:58 the whistlers are observed to increase in frequency once they have reached the LHR cutoff frequency--or to be "reflected". All long-hop whistlers from then on to 0626:25 are observed to be reflected at the LHR cutoff frequency. In addition to the sharp lower-frequency cutoff, one notes the reflected whistlers also display an upper-frequency cutoff. Beginning about 0626:45 the whistlers are observed no longer to be cutoff nor reflected but to cause an enhancement at the LHR frequency. This enhancement by each long-hop whistler is observed to occur for the remainder of the

spectrogram. An analysis of the magnetic receiver high-band data shows that a reflected magnetic component is also faintly observed for some of the whistlers. From an analysis of proton whistlers observed in the low-band data of both receivers the hydrogen concentration has been observed to rise from approximately 20% at 0622 to more than 80% by 0628.

A possible explanation for the observed reflection can be discussed using Figure 12. The left-hand portion is an expected profile for the LHR frequency as a function of altitude. The right-hand portion is a frequency-time display of the reflected whistler. Consider the satellite to be near 2500 km. The satellite observes no component in the whistlers below the local f_{LHR} because any frequency component below the local f_{LHR} will be cutoff. Only components in frequency equal to or greater than the f_{LHR} will be observed. Frequencies above the f_{LHR} will be observed twice, once coming down and once after being reflected. The greater the frequency is above f_{LHR} the longer the delay time because the altitude at which that component is reflected is farther below the satellite. At the maximum of f_{LHR} with altitude (near 2000 km in the diagram), f_{LHR} is varying very slowly with altitude. The wave will travel in a region whose local f_{LHR} is near its frequency some time before reaching its reflection

altitude. Near the f_{LHR} the index of refraction is very large and the phase velocity is very small. Thus as the frequency approaches the maximum f_{LHR} for the ionosphere below the satellite, the delay time becomes very long. For frequencies above the maximum f_{LHR} no reflection will occur. We conclude that the lower-frequency cutoff for the reflection phenomena is the f_{LHR} for the ambient plasma near the satellite while the upper frequency cutoff is the maximum f_{LHR} for the ionosphere below the satellite.

Other new LHR phenomena observed on Injun 5 are multiple frequency noise bands. Such a case is shown in Figure 13. Three distinct electric field noise bands are observed including one which has a well defined magnetic field component. The mid-latitude LHR noise band is identifiable from its characteristic form and sharp lower-frequency cutoff. As this lower-cutoff frequency is believed to be at or near the local f_{LHR}, it is evident the other bands are not related to the local f_{LHR}. The merging of the electromagnetic and LHR noise bands at approximately 0815:30 UT and the upper-cutoff frequency for the electromagnetic noise bands suggest that this band could be related to the f_{LHR} at some other altitude by the same process discussed for the reflected whistlers. The appearance of the band in the magnetic receiver data is very similar to the appearance of noise bands in the

Injun 3 VLF data which were thought to be associated with LHR noise bands.

Figure 14 shows another instance of a second noise band moving in frequency away from the LHR noise band. This second band, however, does not have an observable magnetic component. At about 0851:20 UT two reflected whistlers are also observed. Between 0848:40 and 0849:40 UT a "shadow" band is present just below the LHR cutoff frequency. This band is much less intense than the LHR noise band, has a fairly sharp lower-frequency cutoff, and varies in time as the lower-frequency cutoff of the LHR noise band. As yet there is no theory to explain this shadow band.

Another new LHR phenomena observed is the modulation of the lower-frequency cutoff of the LHR noise band at the spin rate of the satellite as shown in Figures 15, 16, and 17. Figure 15 shows an electric receiver spectrogram for revolution 78 when the satellite was spinning fairly rapidly. Below the spectrogram is a plot of the orientation angles of the satellite axes with respect to the magnetic field. The lower cutoff of the LHR noise band is seen to vary periodically at the spin rate of the satellite. The amplitude of each individual variation appears to vary as A cos θ where θ is an orientation angle and A is the amplitude. However,

A is not constant but alternates between two values, one nearly twice the other. The dotted lines show that the nulls in the variation occur for $\theta_x \simeq 0°$ or 180° and $\theta_z \simeq 90°$. A "small" variation follows the magnetic field being in the positive x direction (which is parallel to the magnetic boom) and a "large" variation follows the magnetic field being in the negative x direction. Toward the end of the spectrogram as the LHR noise band becomes more intense, the variation decreases greatly in intensity and vanishes.

Figure 16 is for revolution 162 for which the satellite had approximately the same spin rate as for revolution 78. Again the spin modulation has exactly the same characteristics. The modulation is approximately a cosine function of an orientation angle with alternating amplitudes, a large amplitude modulation following $\theta_x \cong 180°$ and a small amplitude following $\theta_x \cong 0°$. It is also clear the more intense the LHR noise band, the less intense the spin modulation.

Figure 17 is for revolution 1101 when the spin rate was much less than the previous two cases. Again the modulation occurs at the spin rate of the satellite with nulls occurring for $\theta_x \simeq 0°$ or 180° and $\theta_z \cong 90°$. Beginning at 0826:00 UT one modulation appears to be an increase in the lower-frequency cutoff. The

modulation that lowers the cutoff frequency also appears to be banded as can be noted at 0825, 0828, and 0830 UT. Banding can also be seen for revolution 162 in Figure 16 at 0530:50.

Figure 18 is a plot of the occurrence of spin modulation of the LHR noise bands as a function of altitude and INV. Spin modulation was never observed when the LHR cutoff frequency was below 7 kHz. As INV decreases, f_{LHR} increases. Thus as the plot shows, the occurrence of spin modulation corresponds to lower INV. Comparing the spin modulation occurrence to the measured LHR occurrence (Figure 9) we see that typically spin modulation occurs at lower INV than measured LHR and also the occurrence of the two phenomena is usually not simultaneous. These general results agree well with the three cases illustrated. The large gap in the occurrence of spin modulation at low INV and low altitude has two plausible explanations. At low altitude and low INV the LHR cutoff frequency is probably enough above 10 kHz, the upper-cutoff frequency of the receivers, that the spin modulation usually will not be seen. Also at low altitudes the electric receivers saw considerable interference that could dominate the spectrograms to the extent the spin modulation could not be seen if it were present.

The characteristics of the receivers probably explain why the spin modulation decreases in intensity and eventually disappears when the LHR noise band enters the spectrogram. A large signal in the receivers will tend to suppress a smaller signal. When the noise band is above the upper frequency limit of the receivers, the spin modulation below 10 kHz might be the strongest signal and thus would be present. When the noise band drops below 10 kHz the spin modulation intensity is suppressed because the noise band intensity is much greater. Frequently we see only the spin modulation and no noise band, presumably because the LHR frequency is above 10 kHz.

A possible explanation for the spin modulation of the LHR cutoff frequency is the doppler shift effect. Since the doppler shift, $\Delta\omega = \vec{k} \cdot \vec{v}$, is dependent on the wave number ($\vec{k}$) direction, the observed spin modulation may be due to the rotating antenna pattern picking out waves from different directions as the satellite rotates. The characteristics of the spin modulation tend to support this explanation. The modulation varies approximately as cos θ (where θ is an orientation angle) and $\Delta\omega = kv \cos \theta'$, where θ' is the angle between $\vec{k}$ and $\vec{v}$. The maximum modulation observed was approximately $\Delta f = 1$ kHz at $f = 8$ kHz. The velocity of the satellite varies from 6 to 8 km/sec. The wavelength of

the spin modulation is thus seen to be

$$\lambda = \frac{2\pi}{k} = \frac{2\pi\, v}{\Delta\omega} = \frac{2\pi\, v}{2\pi\, \Delta f} = \frac{v}{\Delta f} \approx 6 \text{ to } 8 \text{ meters}$$

which is comparable to the antenna length of 2.85 meters.

The banding of the spin modulations supports the idea of selected wave numbers being observed. The asymmetry of the amplitudes could be explained by the asymmetry of the antenna pattern due to the asymmetry of the satellite structure and booms.

Another possible explanation for the spin modulation is that the LHR noise may be generated by an interaction between the spacecraft and the surrounding plasma. This could introduce an orientation dependence because of the asymmetric shape of the spacecraft body and booms. At the present time the origin of the observed spin modulation is not clearly understood.

Figures 19, 20, and 21 contain spectrograms of electric receiver high-band data for several typical passes. The most striking feature of all the spectrograms is the similarity of the LHR noise bands observed. For revolution 53 in Figure 19, the noise band from 0415:30 UT to 0422:00 UT is of the mid-latitude type. The lower-cutoff frequency is seen to decrease as INV increases. From 0420 to 0421 a shadow band is observed. At

63° INV the LHR activity vanishes and then returns near 65° INV at 0423 as the polar type. Revolution 54, two hours later, has very similar characteristics but also has spin modulation in the first minute of data. The mid-latitude LHR noise vanishes abruptly at 0620 and 65° INV. Revolution 115 has approximately four minutes of spin-modulated LHR noise at the beginning of the spectrogram. Revolutions 115 and 116 show that for a separation in altitude of slightly less than 100 km and in time of about two hours, the LHR bands are very similar and very close in the frequency of the lower cutoff for the same point in space. For revolution 211, a very strong shadow band is observed at 0402 UT.

In Figure 20, revolution 225 shows a transition from mid-latitude LHR noise to noise having no cutoff to polar-type LHR noise. For revolution 272, a strong shadow band is observed from 0424 UT to 0425 UT. Spin modulation is faintly observed in the first three minutes of the data. For revolution 332, we observe spin modulation in the first four and one-half minutes of data. We see that it decreases in intensity as the LHR noise band becomes more intense as it decreases in frequency into the receiver bandwidth.

In Figure 21, revolution 345 shows a typical transition from mid-latitude LHR noise to background noise at 60° INV and

then to polar LHR noise at 65°. For revolution 370, at 0545 the LHR cutoff frequency is observed to drop more than 4 kHz in less than 20 seconds. In revolution 381, the fluctuations in the LHR cutoff frequency just before 0321 UT and 43° INV are probably due to crossing the plasmapause boundary as has been previously observed by Carpenter et al. [1968]. Revolution 382 is seen to have LHR phenomena similar to the preceding revolution except there is no crossing of the plasmapause boundary. Revolution 749 is observed to have LHR noise increasing with time because it is a southbound pass. All previous examples were northbound passes. As expected, we see that as INV decreases, the LHR cutoff frequency increases. On revolution 749 we also see a strong shadow band between 0950 UT and 0951 UT. All of the above spectrograms show data that is typically observed on most night mid-latitude passes by the Injun 5 VLF electric receiver.

V. CONCLUSIONS

The most important outcome of this study has been the observation of new phenomena which have aided in bringing together past observations and possible explanations for these observations. The reflection phenomena is an experimental observation in agreement with past theory suggesting that some observed LHR noise is due to reflection processes. Multiple bands and the upper cutoff for the reflection phenomena suggest that the characteristics of the LHR noise observed by the satellite are dependent not only on the local f_{LHR} but also on the maximum f_{LHR} with altitude.

Although this study may not have concretely settled any questions, it has offered new evidence to assist in the solution. It has also raised new questions and suggested more possible studies. Further attempts to produce f_{LHR} profiles in altitude should be made by carefully analyzing all the VLF analog data. The time to produce such an analysis is the main obstacle. A study of the characteristics of spin modulation in the southern hemisphere is in order. It would also be of interest to develop models and the necessary theory to do quantitative calculations on the time delay for reflected whistlers to determine the altitude of the maximum f_{LHR}. A useful calculation would also be to

determine f_{LHR} from knowing f_o, the cutoff frequency, and the power spectrum. From f_{LHR}, concentrations from measurements on ion whistlers, and number density from the AFCRL experiment on Injun 5, a fairly accurate model of the ionosphere could be determined. Thus this study is really only a beginning.

REFERENCES

Barrington, R. E., and J. S. Belrose, Preliminary results from the very-low-frequency receiver aboard Canada's Alouette satellite, Nature, 198, 651, 1963.

Barrington, R. E., J. S. Belrose, and D. A. Keeley, Very-low-frequency noise bands observed by the Alouette 1, J. Geophys. Res., 68, 6539, 1963.

Belrose, J. S., and R. E. Barrington, VLF noise bands observed by the Alouette 1 satellite, Radio Sci., 69D, 69, 1965.

Brice, N. M., and R. L. Smith, A very-low-frequency plasma resonance, Nature, 203, 926, 1964.

Brice, N. M., and R. L. Smith, Lower hybrid resonance emissions, J. Geophys. Res., 70, 71, 1965.

Brice, N. M., R. L. Smith, J. S. Belrose, and R. E. Barrington, Triggered very-low-frequency emissions, Nature, 203, 926, 1964.

Carpenter, D. L., F. Walter, R. E. Barrington, and D. J. McEwen, Alouette 1 and 2 observations of abrupt changes in whistler rate and of VLF noise variations at the plasmapause--a satellite ground study, J. Geophys. Res., 73, 2929, 1968.

Gurnett, D. A., G. W. Pfeiffer, R. R. Anderson, S. R. Mosier, and D. P. Cauffman, Initial observations of VLF electric and magnetic fields with the Injun 5 satellite, Department of Physics and Astronomy, The University of Iowa, Research Report 69-19, 1969.

Jensen, D. C., and J. C. Cain, An interim geomagnetic field (abstract), J. Geophys. Res., 67, 3568, 1962.

Kimura, I., Effects of ions on whistler-mode ray tracing, Radio Science, 1, (3) (new series), 269, 1966.

Laaspere, T., M. G. Morgan, and W. C. Johnson, Proc. IEEE, 51, 554, 1963.

Laaspere, T., M. G. Morgan, and W. C. Johnson, Observations of lower hybrid resonance phenomena on the OGO 2 spacecraft, J. Geophys. Res., 74, 141, 1969.

McEwen, D. J., and R. E. Barrington, Some characteristics of the lower hybrid resonance noise bands observed by the Alouette 1 satellite, Can. J. Phys., 45, 13, 1967.

Shawhan, S. D., Behavior of VLF ray paths in the ionosphere, Department of Physics and Astronomy, The University of Iowa, Research Report 67-25, 1967.

Smith, R. L., and N. M. Brice, Propagation in multicomponent plasmas, J. Geophys. Res., 69, 5029, 1964.

Smith, R. L., I. Kimura, J. Vigenon, and J. Katsufrakis, Lower hybrid resonance noise and a new ionospheric duct, J. Geophys. Res., 71, 1925, 1966.

Stix, T. H., The Theory of Plasma Waves, McGraw-Hill Book Company, New York, 1962.

Storey, L. R. O., Antenna electrique dipole pour reception TBF dans l'ionosphere, L'onde Electrique, 45, 1427, 1965.

Storey, L. R. O., and J. C. Cerisier, An interpretation of the noise bands observed near the lower hybrid resonance frequency by artificial satellites, C. R. Acad. Sc. Paris, t.266, 525, 1968.

Thorne, R. M., and C. F. Kennel, Quasi-trapped VLF propagation in the outer magnetosphere, J. Geophys. Res., 72, 857, 1967.

F I G U R E S

Figure 1. Variation of LHR frequency and refractive index with altitude, following Smith et al. [1966].

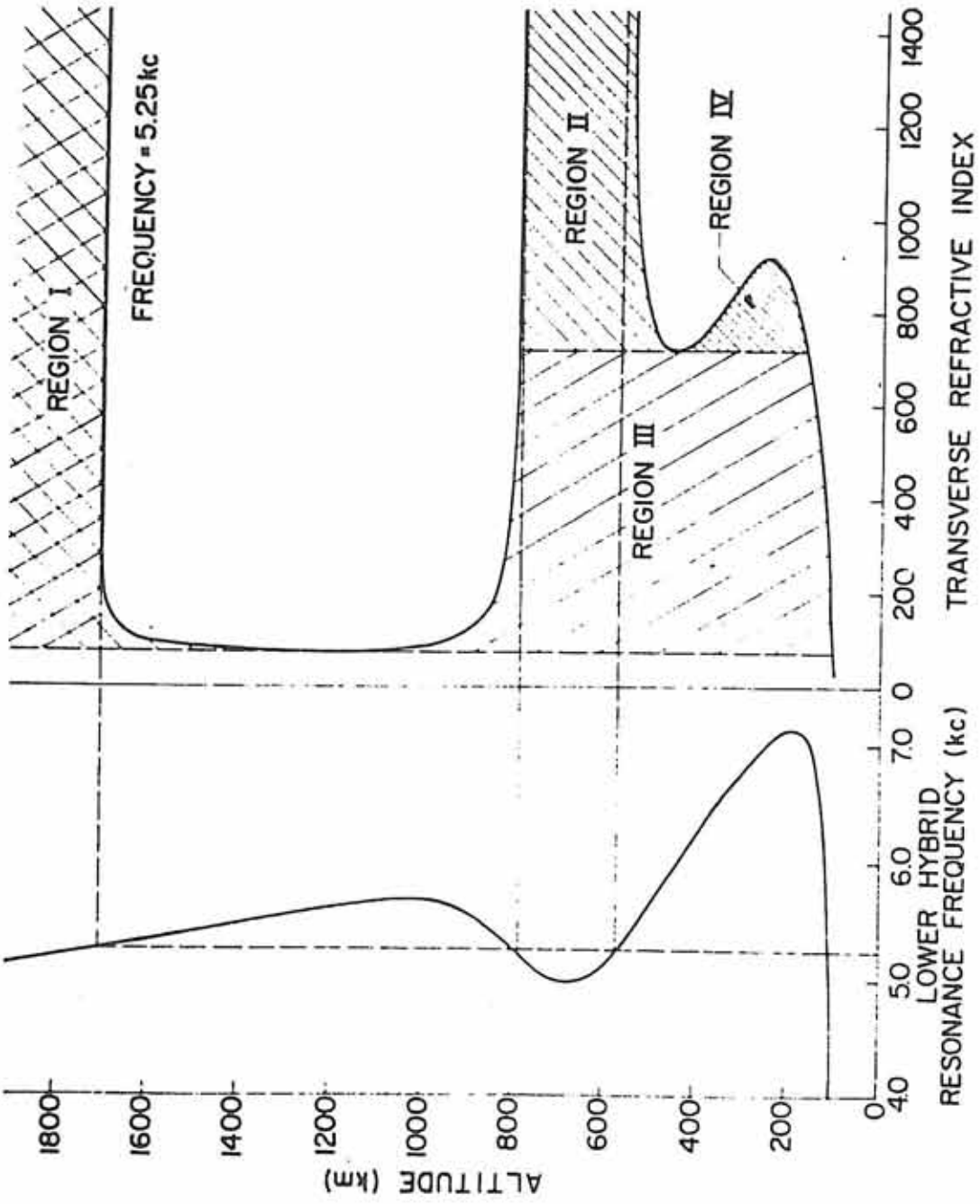
REGION I
FREQUENCY = 5.25kc
REGION II
REGION III
REGION IV
ALTITUDE (km)
1800
1600
1400
1200
1000
800
600
400
200
0
40
5.0
6.0
7.0
0
200
400
600
800
1000
1200
1400
LOWER HYBRID RESONANCE FREQUENCY (kc)
TRANSVERSE REFRACTIVE INDEX

Figure 2. Typical wave path near f_{LHR}.

A-G69-264

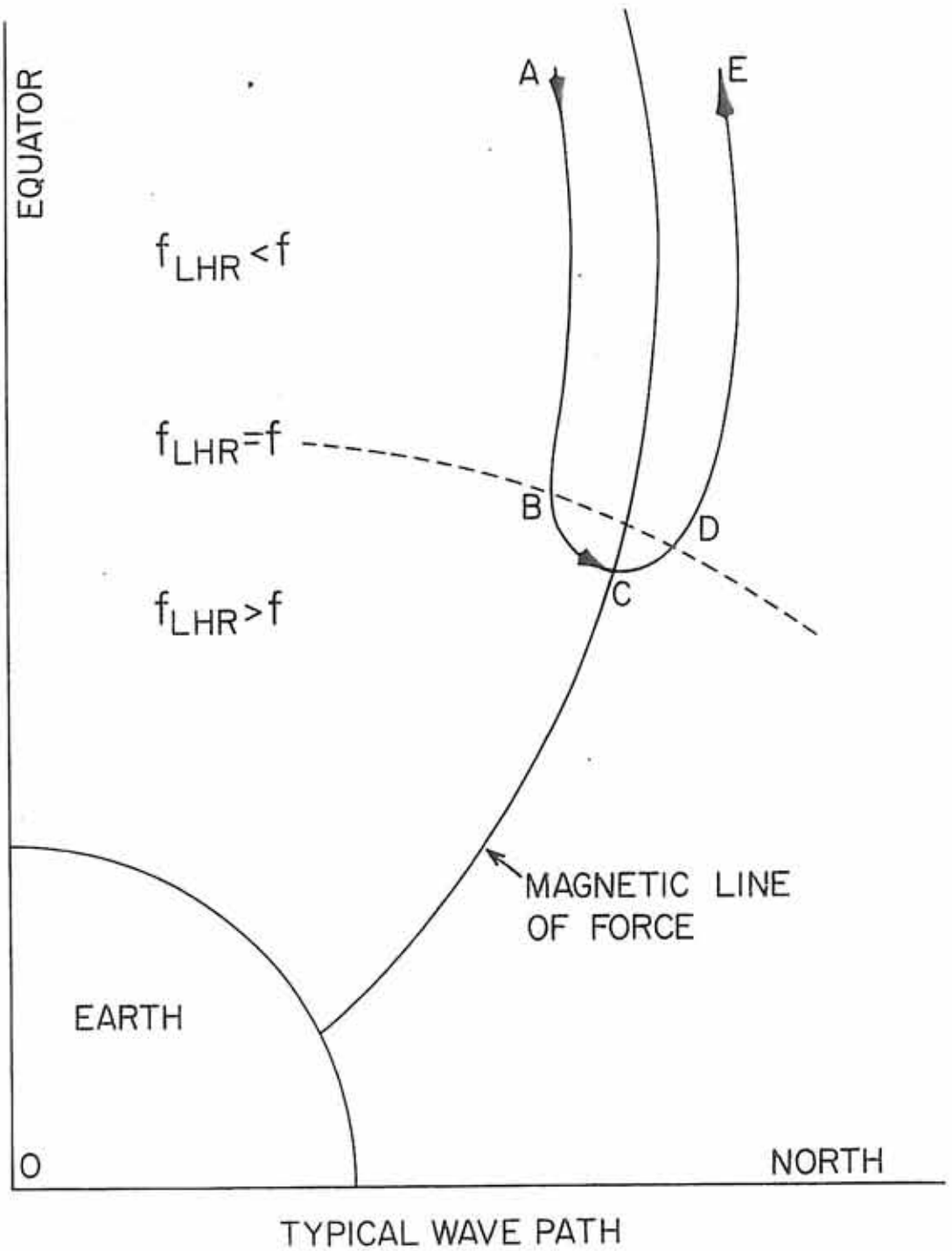

TYPICAL WAVE PATH

Figure 3. Index of refraction surface near f_{LHR}.

A-G69-263

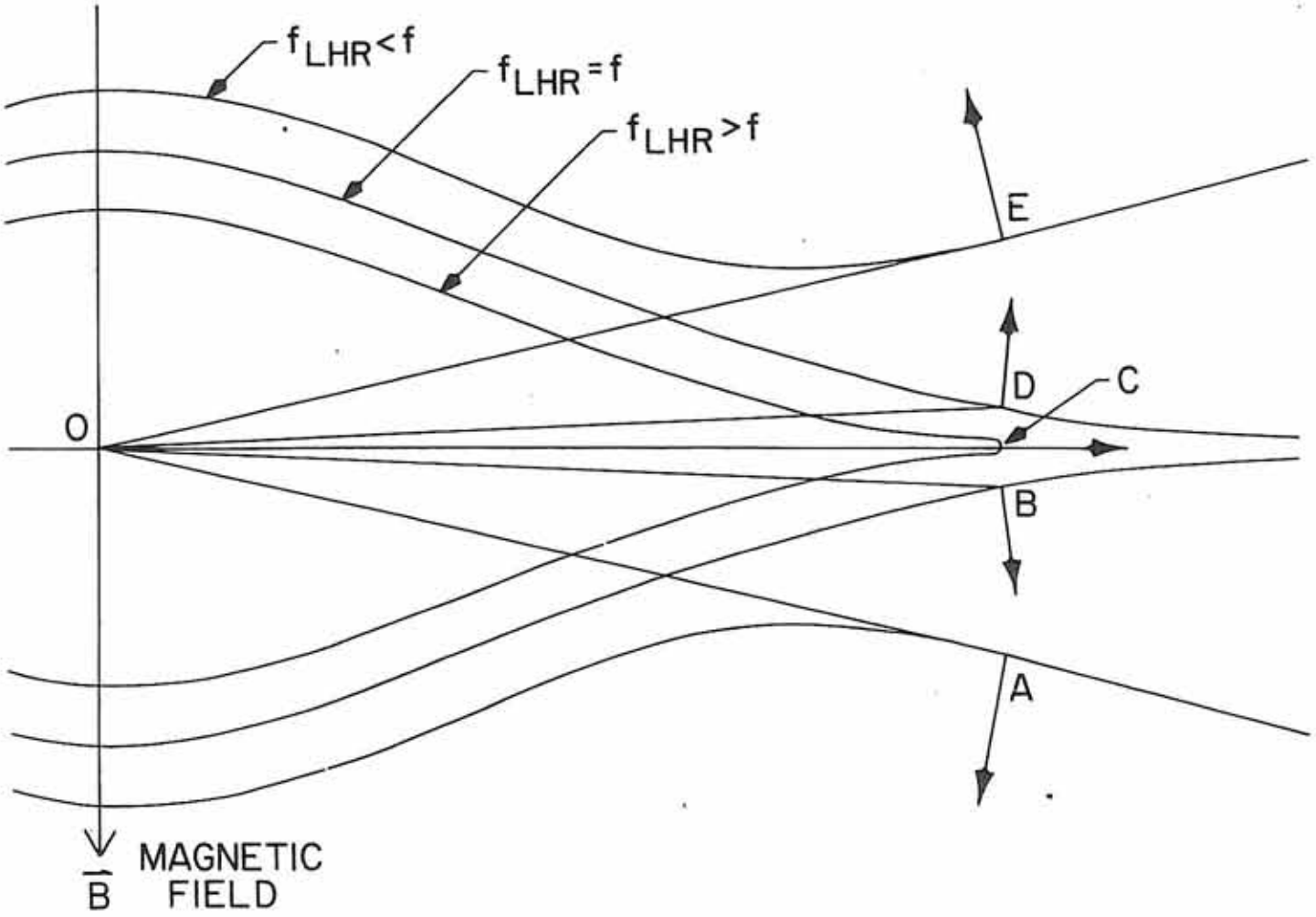

REFRACTIVE INDEX SURFACES

Figure 4. Power spectrum near f_{LHR}, following Storey and Cerisier [1968].

A-G69-265

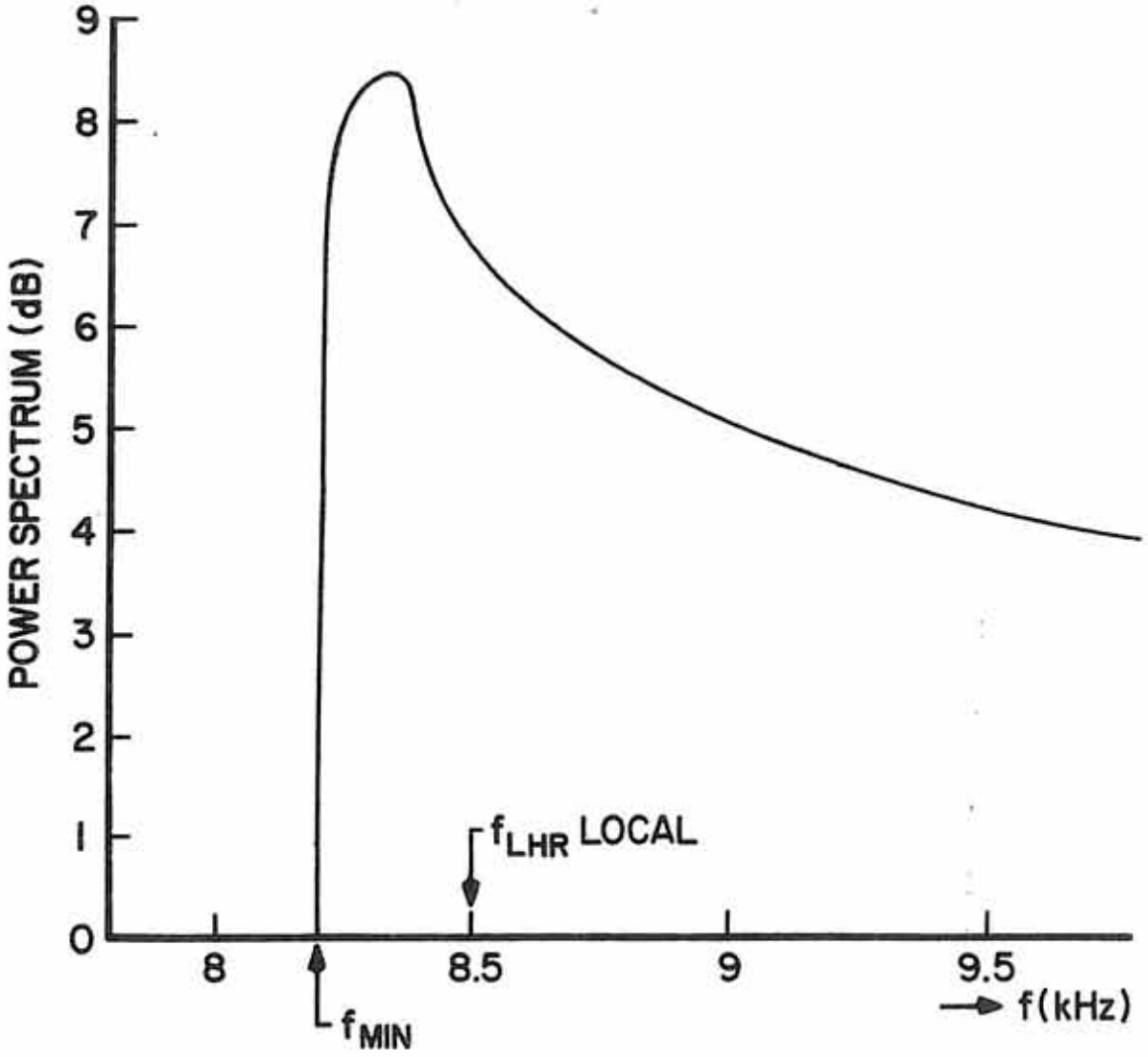

LHR POWER SPECTRUM

Figure 5. Refractive index versus frequency for multicomponent plasma.

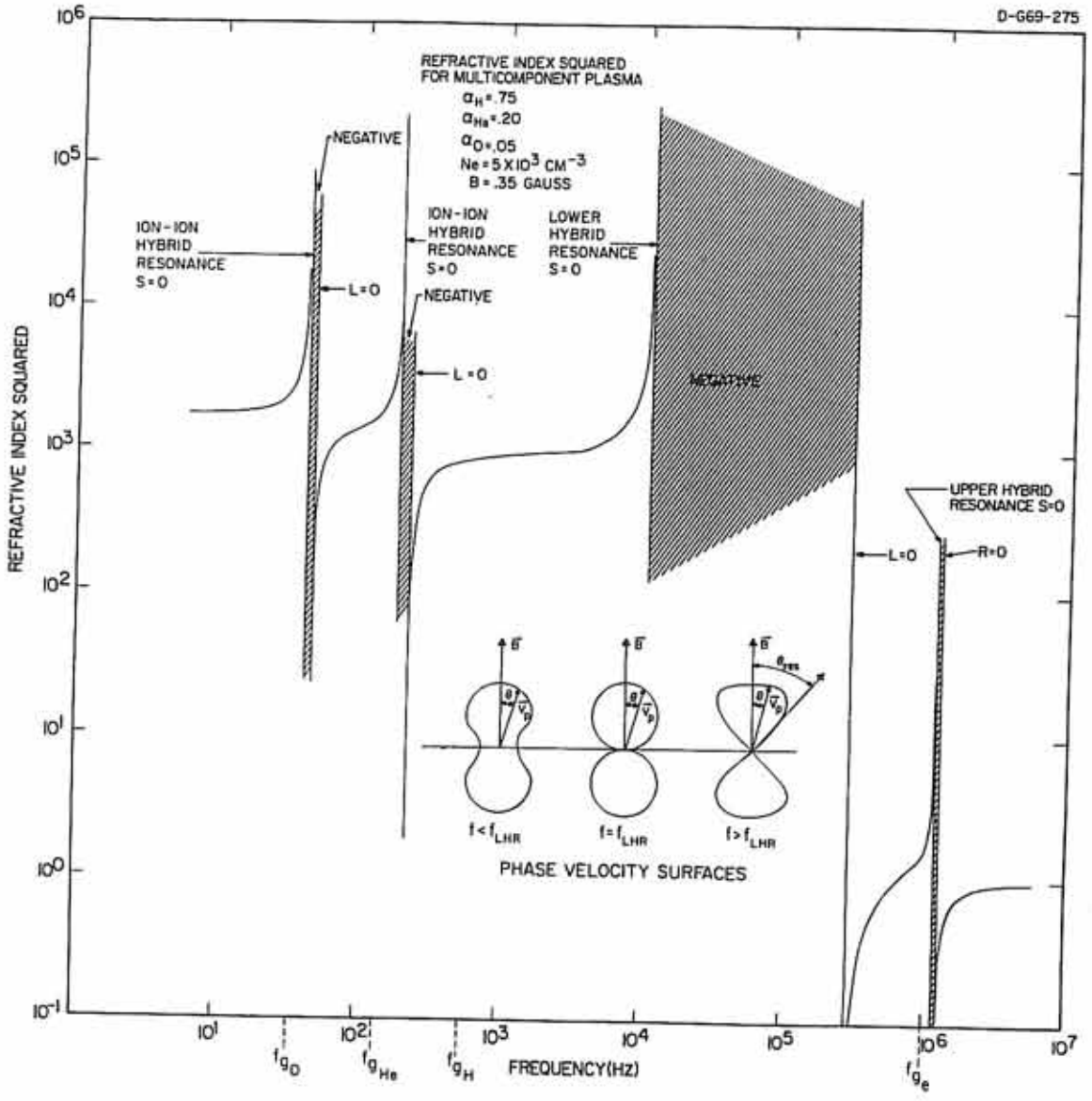
D-G69-275
REFRACTIVE INDEX SQUARED FOR MULTICOMPONENT PLASMA
α_H = .75
α_{He} = .20
α_O = .05
Ne = 5 X 10^3 CM^{-3}
B = .35 GAUSS
NEGATIVE
ION-ION HYBRID RESONANCE S=0
L=0
ION-ION HYBRID RESONANCE S=0
NEGATIVE
L=0
LOWER HYBRID RESONANCE S=0
NEGATIVE
UPPER HYBRID RESONANCE S=0
L=0
R=0
$f < f_{LHR}$
$f = f_{LHR}$
$f > f_{LHR}$
PHASE VELOCITY SURFACES
REFRACTIVE INDEX SQUARED
FREQUENCY(HZ)
f_{g_O}
$f_{g_{He}}$
f_{g_H}
f_{g_e}

Figure 6. Injun 5 Explorer spacecraft.

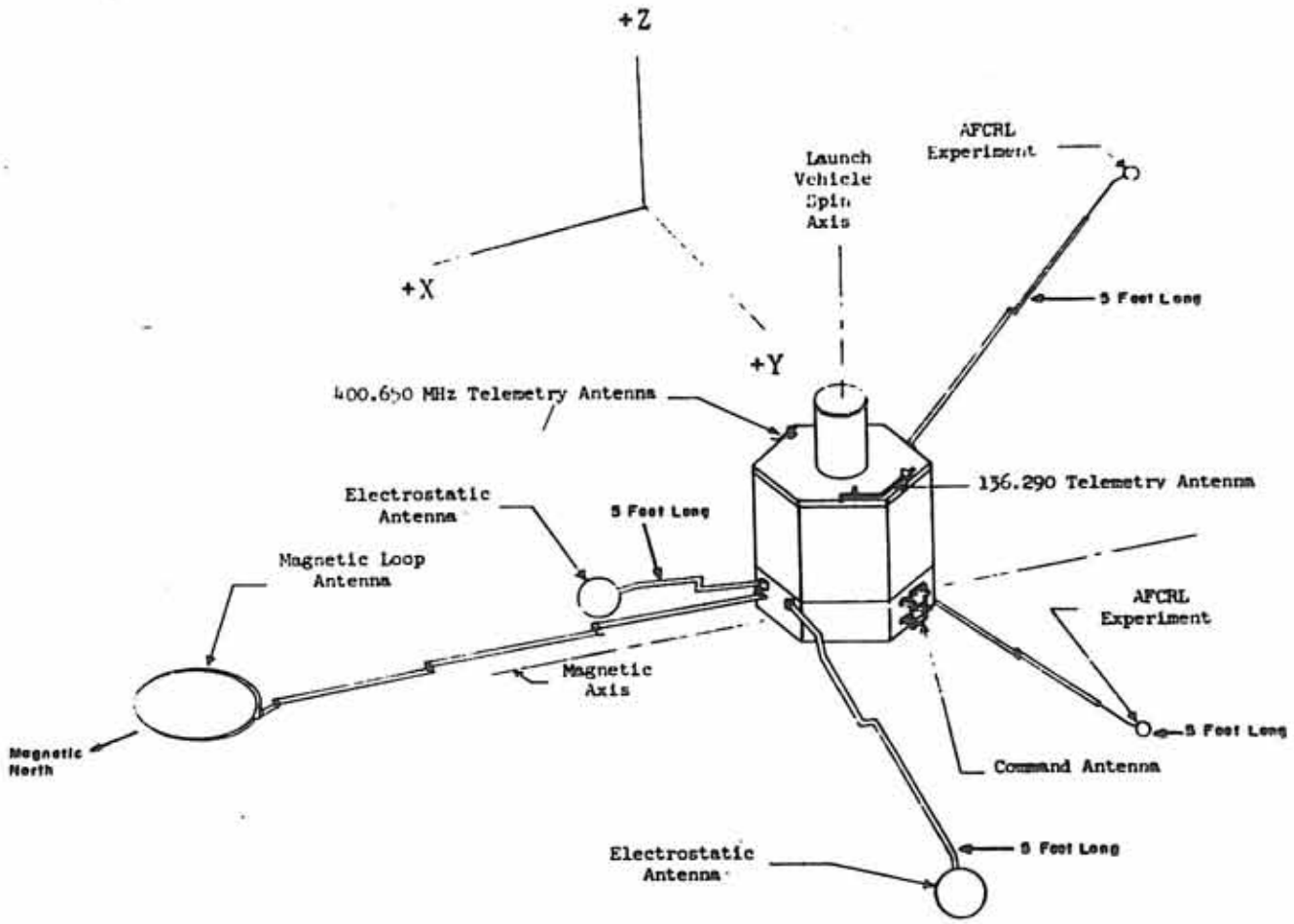

Injun V Explorer Spacecraft

Figure 7. Block diagram of Injun 5 VLF experiment.

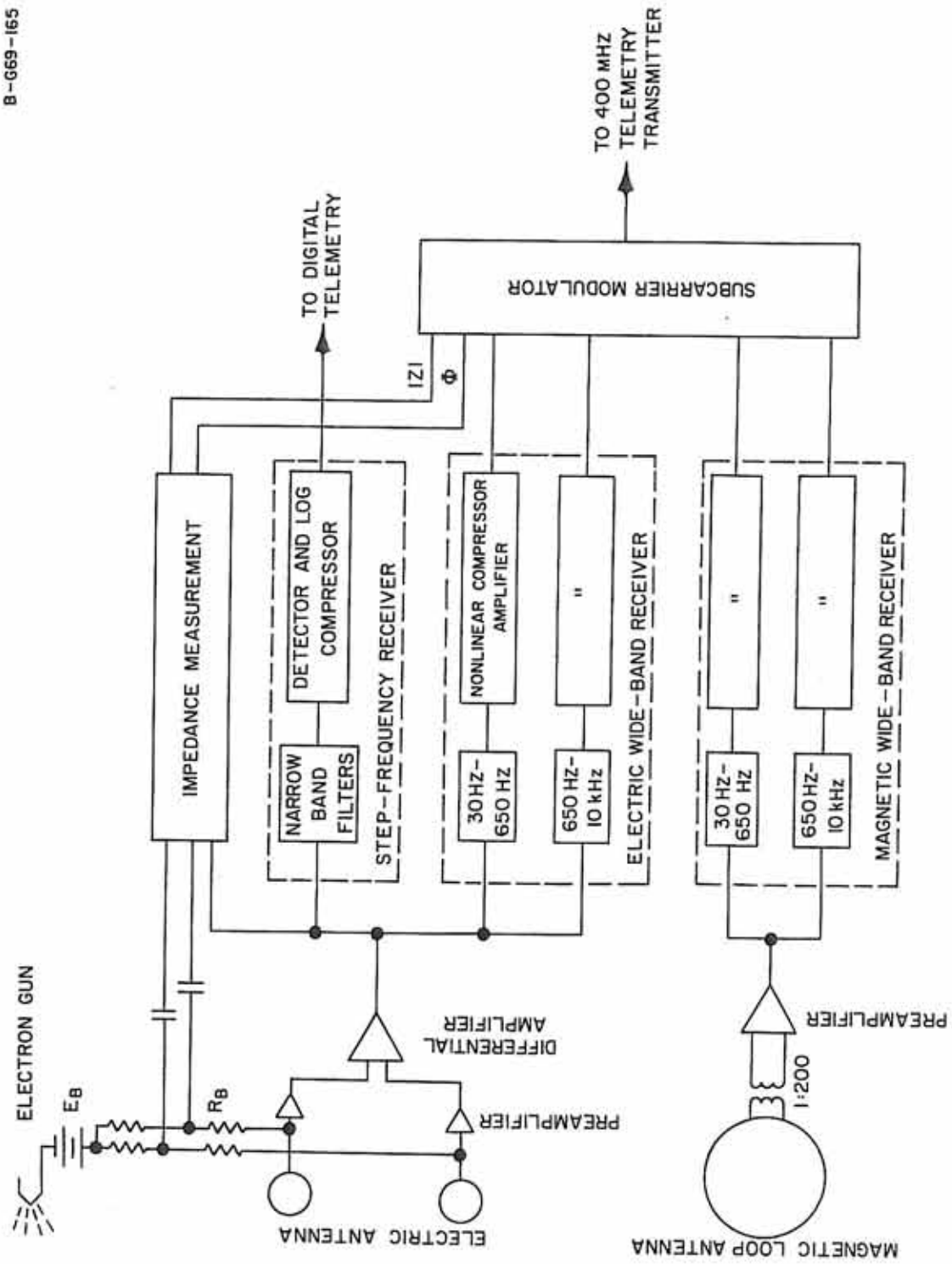
B-G69-165
TO 400 MHZ TELEMETRY TRANSMITTER
TO DIGITAL TELEMETRY
SUBCARRIER MODULATOR
|Z|
Φ
IMPEDANCE MEASUREMENT
STEP-FREQUENCY RECEIVER
NARROW BAND FILTERS
DETECTOR AND LOG COMPRESSOR
ELECTRIC WIDE-BAND RECEIVER
30 HZ-650 HZ
NONLINEAR COMPRESSOR AMPLIFIER
650 HZ-10 kHz
"
MAGNETIC WIDE-BAND RECEIVER
30 HZ-650 HZ
650 HZ-10 kHz
"
"
ELECTRON GUN
E_B
R_B
DIFFERENTIAL AMPLIFIER
PREAMPLIFIER
ELECTRIC ANTENNA
PREAMPLIFIER
1:200
MAGNETIC LOOP ANTENNA

Figure 8. Histogram of measured LHR occurrence versus invariant latitude.

A-G69-268

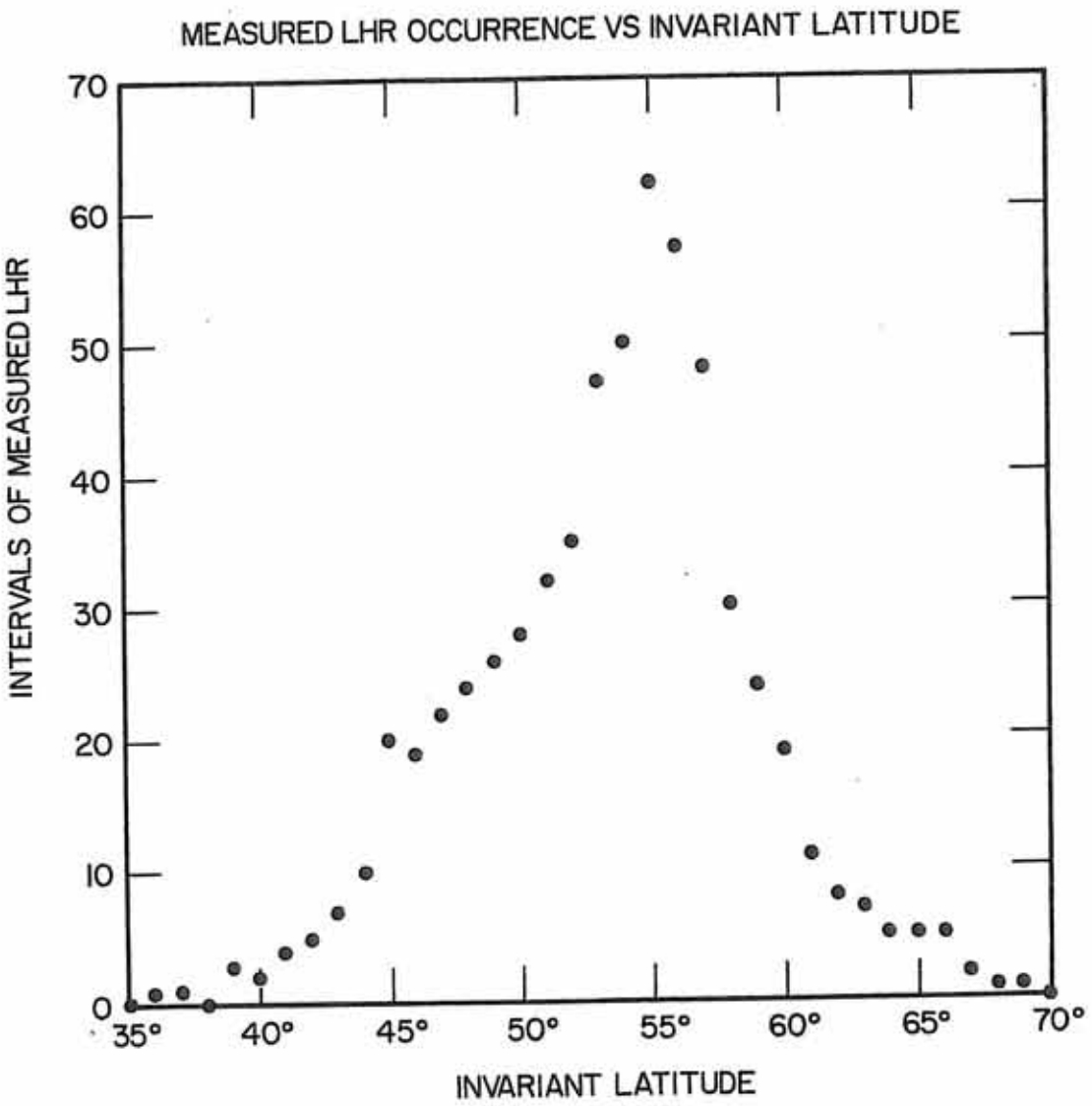
MEASURED LHR OCCURRENCE VS INVARIANT LATITUDE
INTERVALS OF MEASURED LHR
0
10
20
30
40
50
60
70
35°
40°
45°
50°
55°
60°
65°
70°
INVARIANT LATITUDE

Figure 9. Spatial occurrence of measured LHR phenomena.

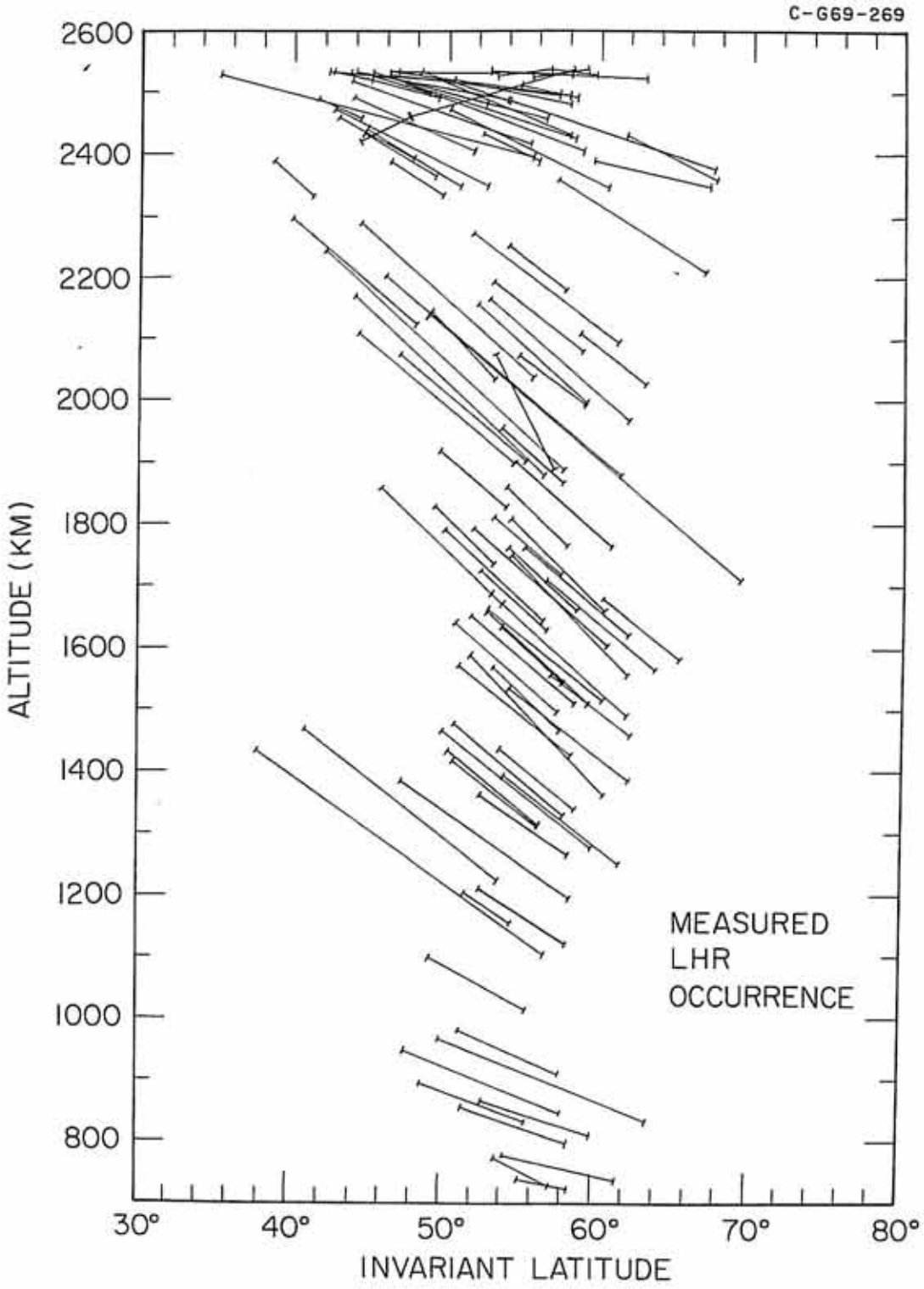
C-G69-269
2600
2400
2200
2000
1800
1600
1400
1200
1000
800
ALTITUDE (KM)
30°
40°
50°
60°
70°
80°
INVARIANT LATITUDE
MEASURED
LHR
OCCURRENCE

Figure 10. LHR cutoff frequency versus altitude for 55° INV.

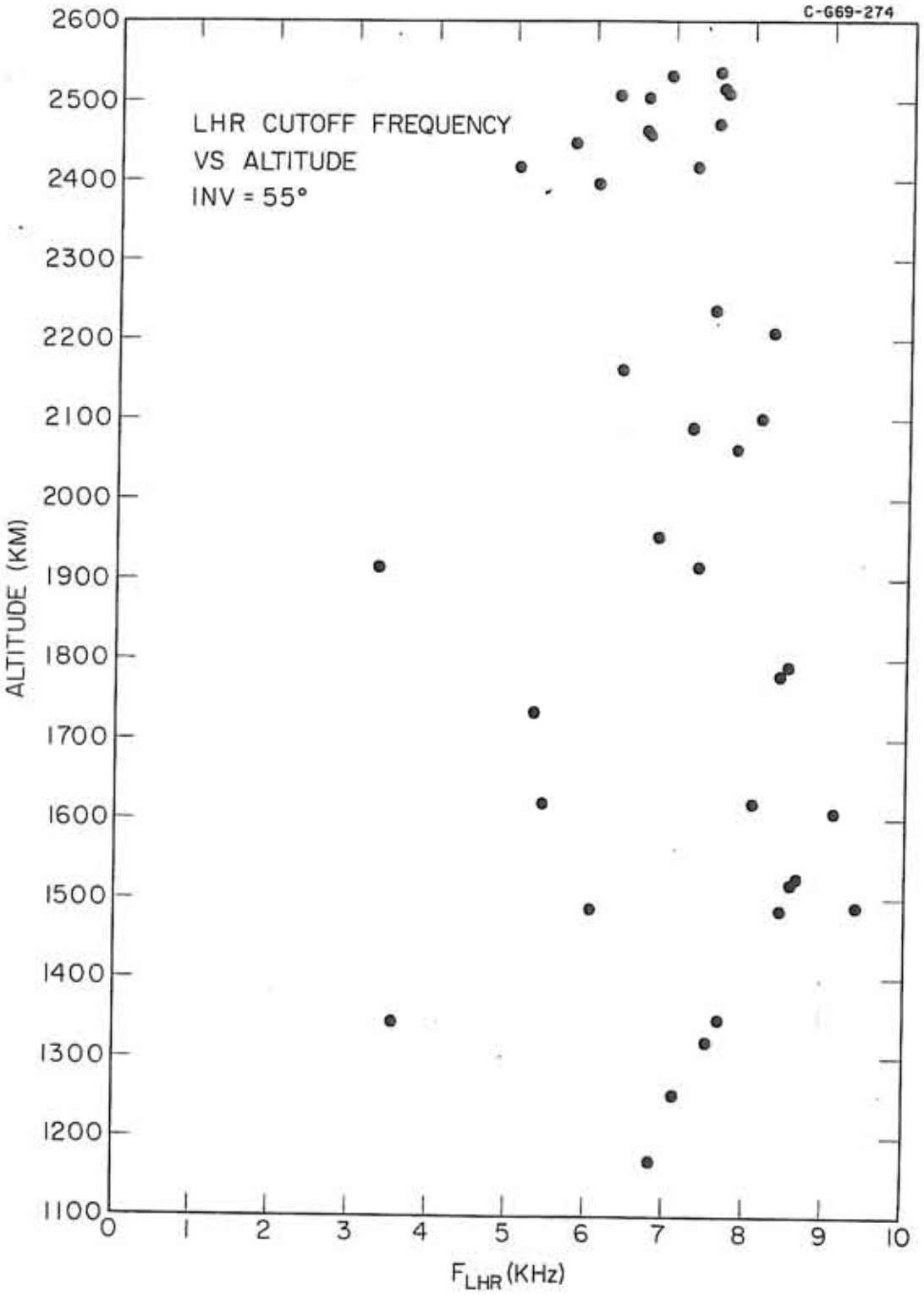
C-669-274
LHR CUTOFF FREQUENCY
VS ALTITUDE
INV = 55°
ALTITUDE (KM)
2600
2500
2400
2300
2200
2100
2000
1900
1800
1700
1600
1500
1400
1300
1200
1100
0
1
2
3
4
5
6
7
8
9
10
F_{LHR} (KHz)

Figure 11. Spectrogram of revolution 1173 reflection phenomena.

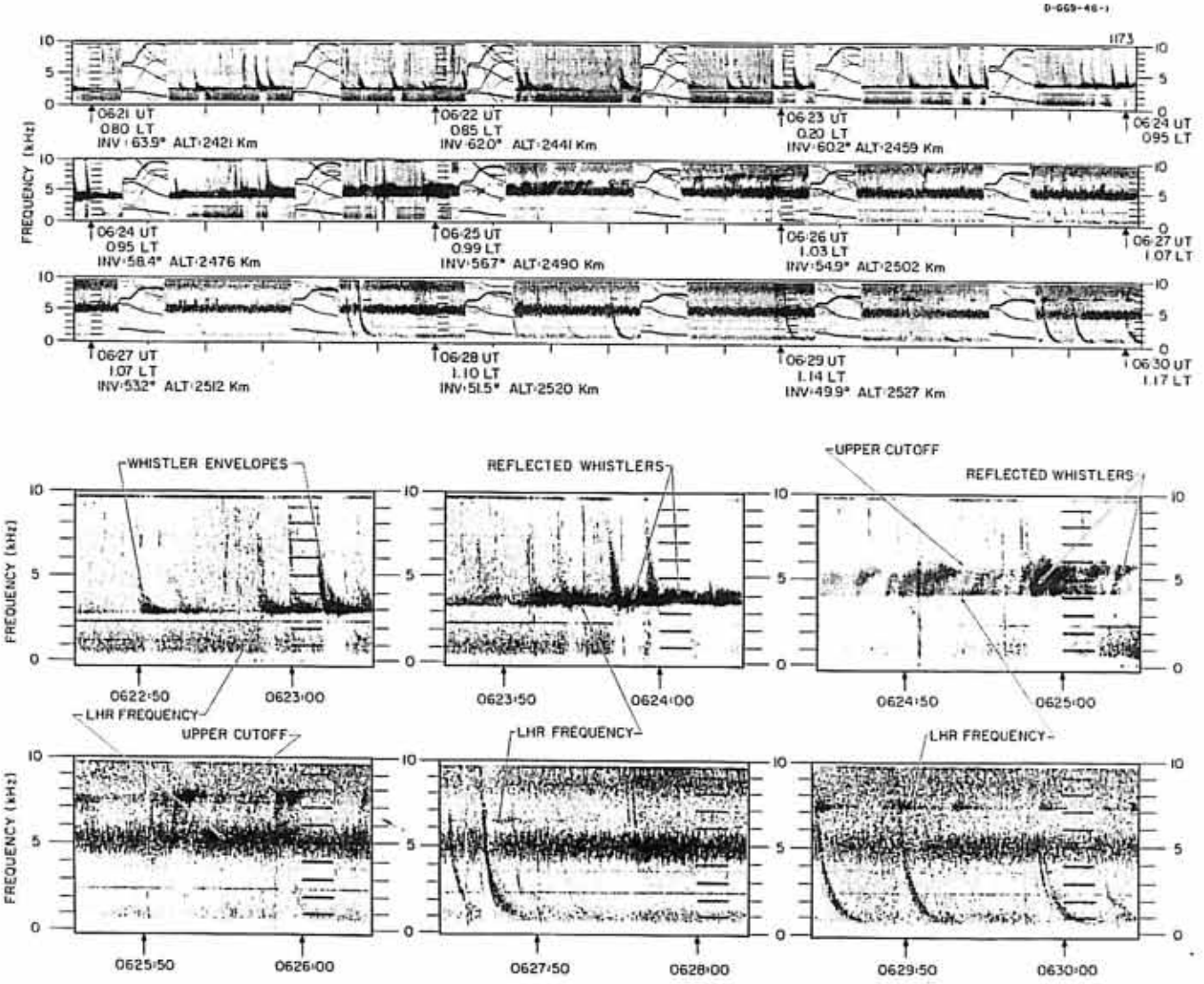
FREQUENCY (kHz)
06·21 UT
0·80 LT
INV·63·9° ALT·2421 Km
06·22 UT
0·85 LT
INV·62·0° ALT·2441 Km
06·23 UT
0·20 LT
INV·60·2° ALT·2459 Km
06·24 UT
0·95 LT
06·24 UT
0·95 LT
INV·58·4° ALT·2476 Km
06·25 UT
0·99 LT
INV·56·7° ALT·2490 Km
06·26 UT
1·03 LT
INV·54·9° ALT·2502 Km
06·27 UT
1·07 LT
06·27 UT
1·07 LT
INV·53·2° ALT·2512 Km
06·28 UT
1·10 LT
INV·51·5° ALT·2520 Km
06·29 UT
1·14 LT
INV·49·9° ALT·2527 Km
06·30 UT
1·17 LT
WHISTLER ENVELOPES
REFLECTED WHISTLERS
UPPER CUTOFF
REFLECTED WHISTLERS
LHR FREQUENCY
UPPER CUTOFF
LHR FREQUENCY
LHR FREQUENCY
0622·50
0623·00
0623·50
0624·00
0624·50
0625·00
0625·50
0626·00
0627·50
0628·00
0629·50
0630·00

Figure 12. Model LHR profile and model reflection phenomenon.

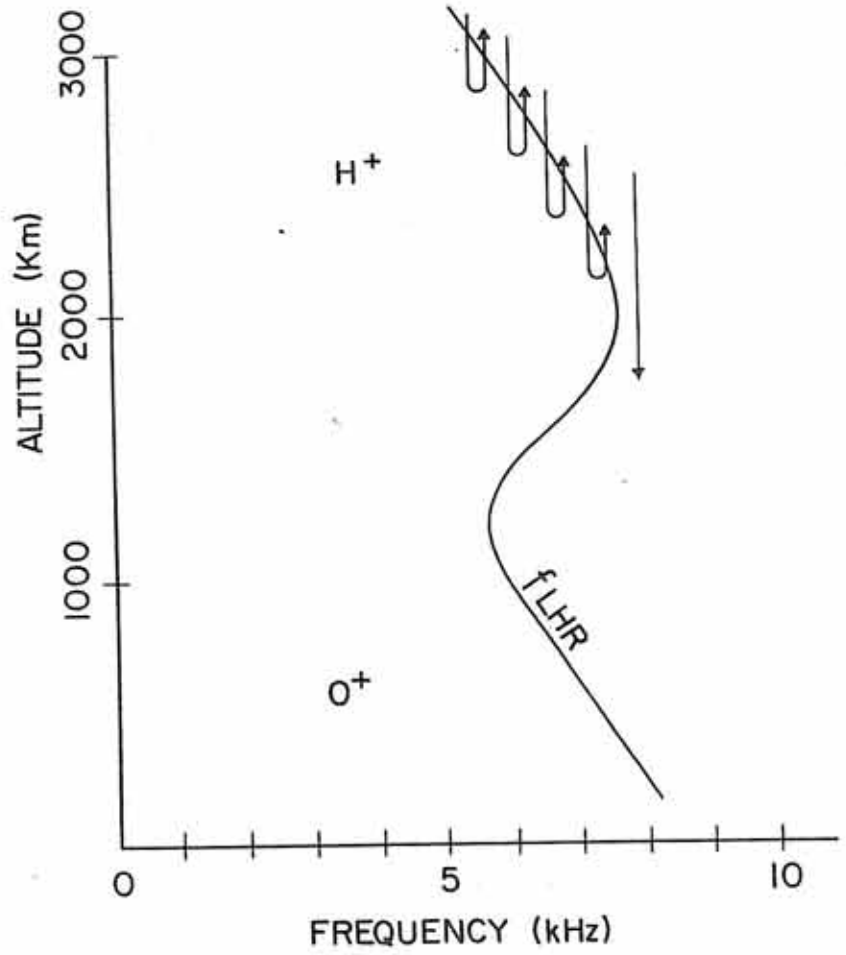
ALTITUDE (Km)
3000
2000
1000
H+
O+
fLHR
0
5
10
FREQUENCY (kHz)

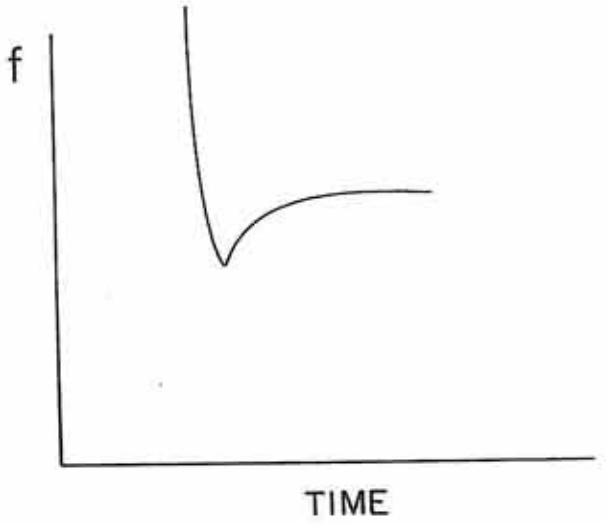
f
TIME

Figure 13. Spectrogram of revolution 55 showing multiple bands.

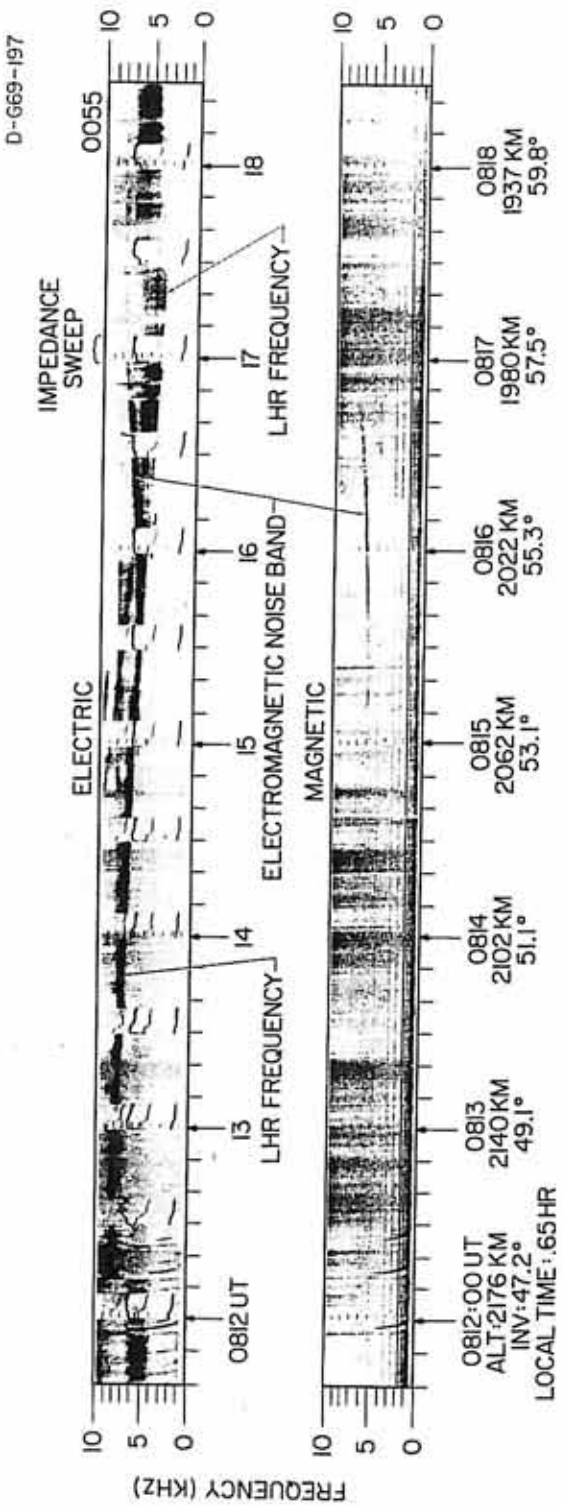
D-669-197
IMPEDANCE SWEEP
0055
ELECTRIC
MAGNETIC
LHR FREQUENCY
ELECTROMAGNETIC NOISE BAND
LHR FREQUENCY
0812 UT
0812:00 UT
ALT:2176 KM
INV:47.2°
LOCAL TIME:.65 HR
0813 2140 KM 49.1°
0814 2102 KM 51.1°
0815 2062 KM 53.1°
0816 2022 KM 55.3°
0817 1980 KM 57.5°
0818 1937 KM 59.8°
FREQUENCY (KHZ)

Figure 14. Spectrogram of revolution 712 showing multiple bands.

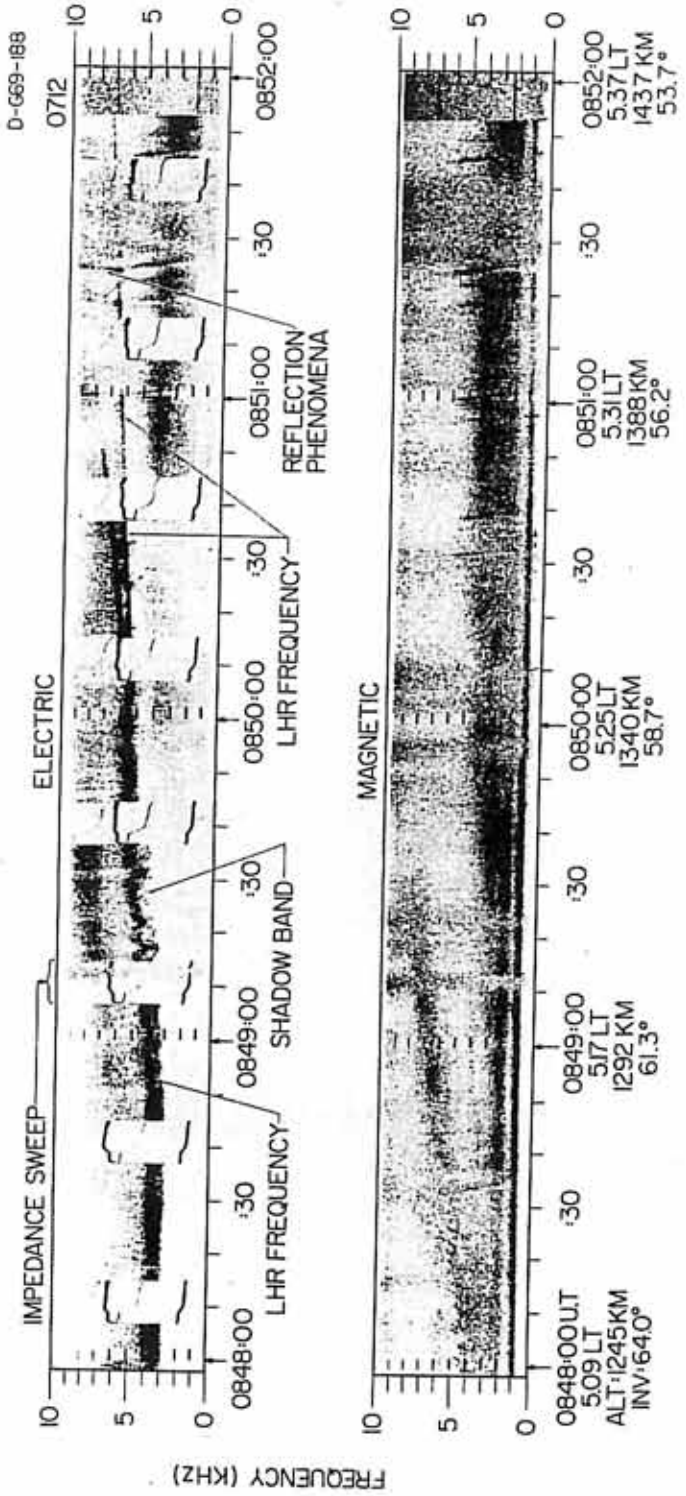
D-669-188
0712
ELECTRIC
IMPEDANCE SWEEP
LHR FREQUENCY
SHADOW BAND
REFLECTION PHENOMENA
LHR FREQUENCY
0848:00
:30
0849:00
:30
0850:00
:30
0851:00
:30
0852:00
MAGNETIC
0848:00 U.T
5.09 LT
ALT: 1245 KM
INV: 64.0°
0849:00
5.17 LT
1292 KM
61.3°
0850:00
5.25 LT
1340 KM
58.7°
0851:00
5.31 LT
1388 KM
56.2°
0852:00
5.37 LT
1437 KM
53.7°
FREQUENCY (KHZ)
10
5
0

Figure 15. Spectrogram of revolution 78 showing spin modulation.

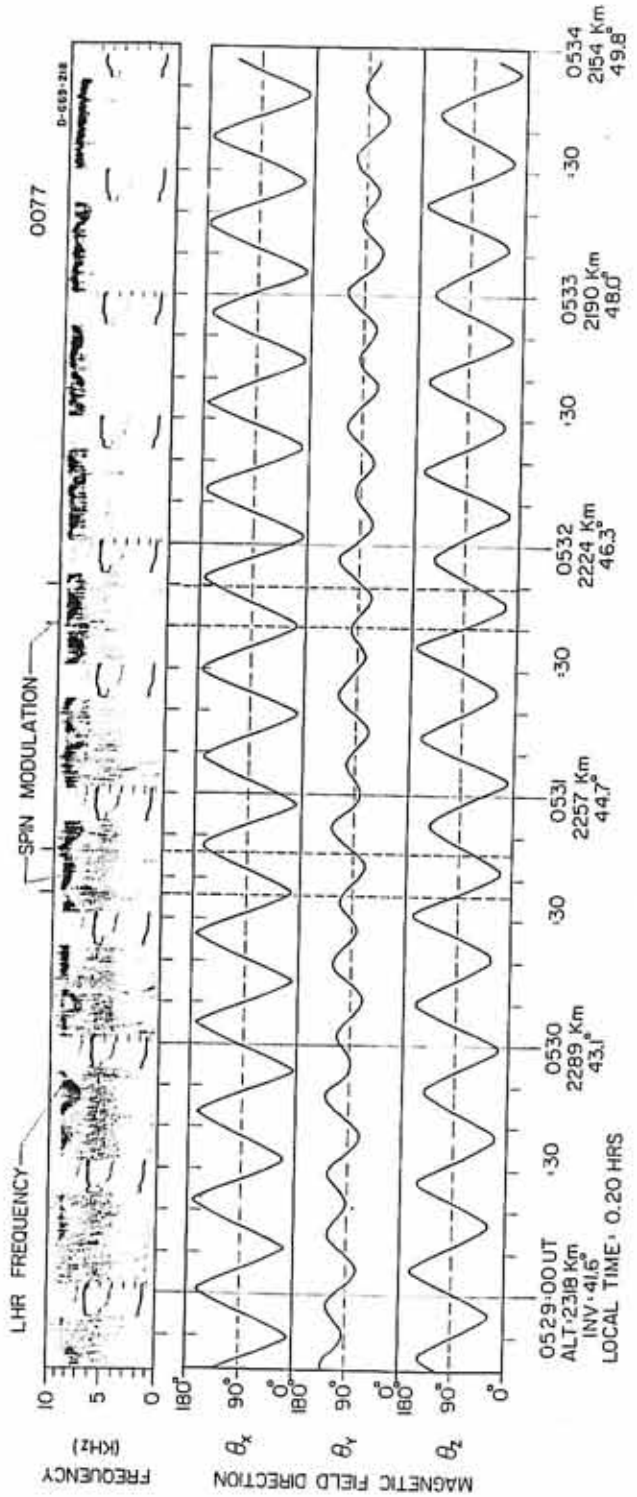
0077
LHR FREQUENCY
SPIN MODULATION
FREQUENCY (KHz)
10
5
0
MAGNETIC FIELD DIRECTION
θ_x
θ_y
θ_z
180°
90°
0°
0529:00 UT
ALT: 2318 Km
INV: 41.6°
LOCAL TIME: 0.20 HRS
:30
0530
2289 Km
43.1°
:30
0531
2257 Km
44.7°
:30
0532
2224 Km
46.3°
:30
0533
2190 Km
48.0°
:30
0534
2154 Km
49.8°

Figure 16. Spectrogram of revolution 162 showing spin modulation.

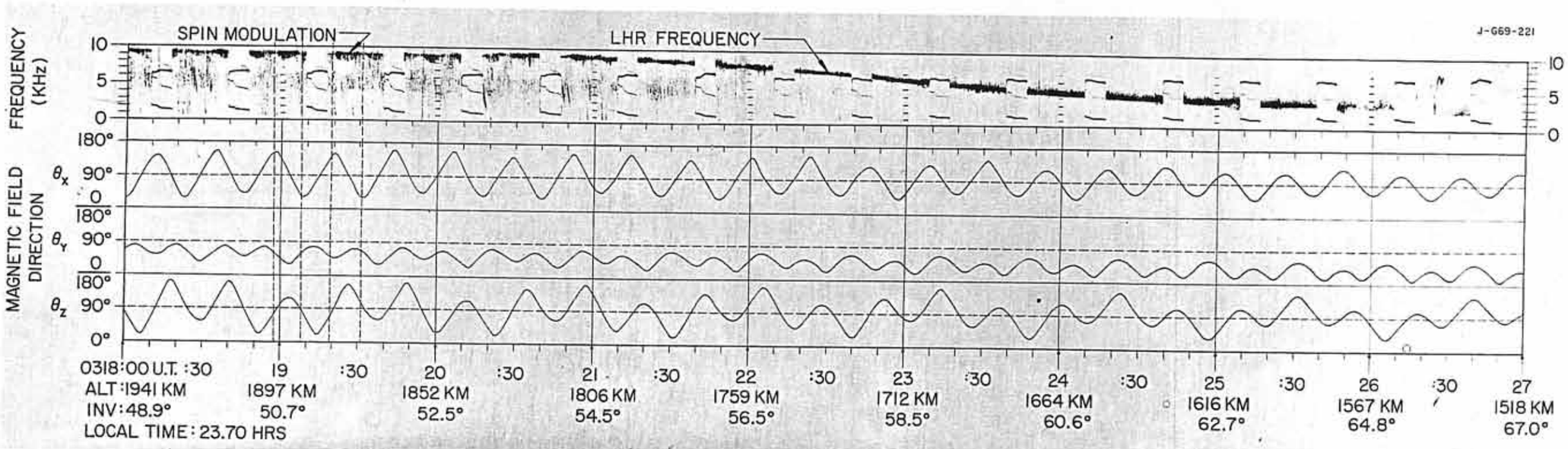
J-G69-221
SPIN MODULATION
LHR FREQUENCY
FREQUENCY (KHz)
10
5
0
MAGNETIC FIELD DIRECTION
180°
θx 90°
0
180°
θy 90°
0
180°
θz 90°
0°
0318:00 U.T. :30
ALT:1941 KM
INV:48.9°
LOCAL TIME: 23.70 HRS
19
1897 KM
50.7°
20
1852 KM
52.5°
21
1806 KM
54.5°
22
1759 KM
56.5°
23
1712 KM
58.5°
24
1664 KM
60.6°
25
1616 KM
62.7°
26
1567 KM
64.8°
27
1518 KM
67.0°
:30

Figure 17. Spectrogram of revolution 1101 showing spin modulation.

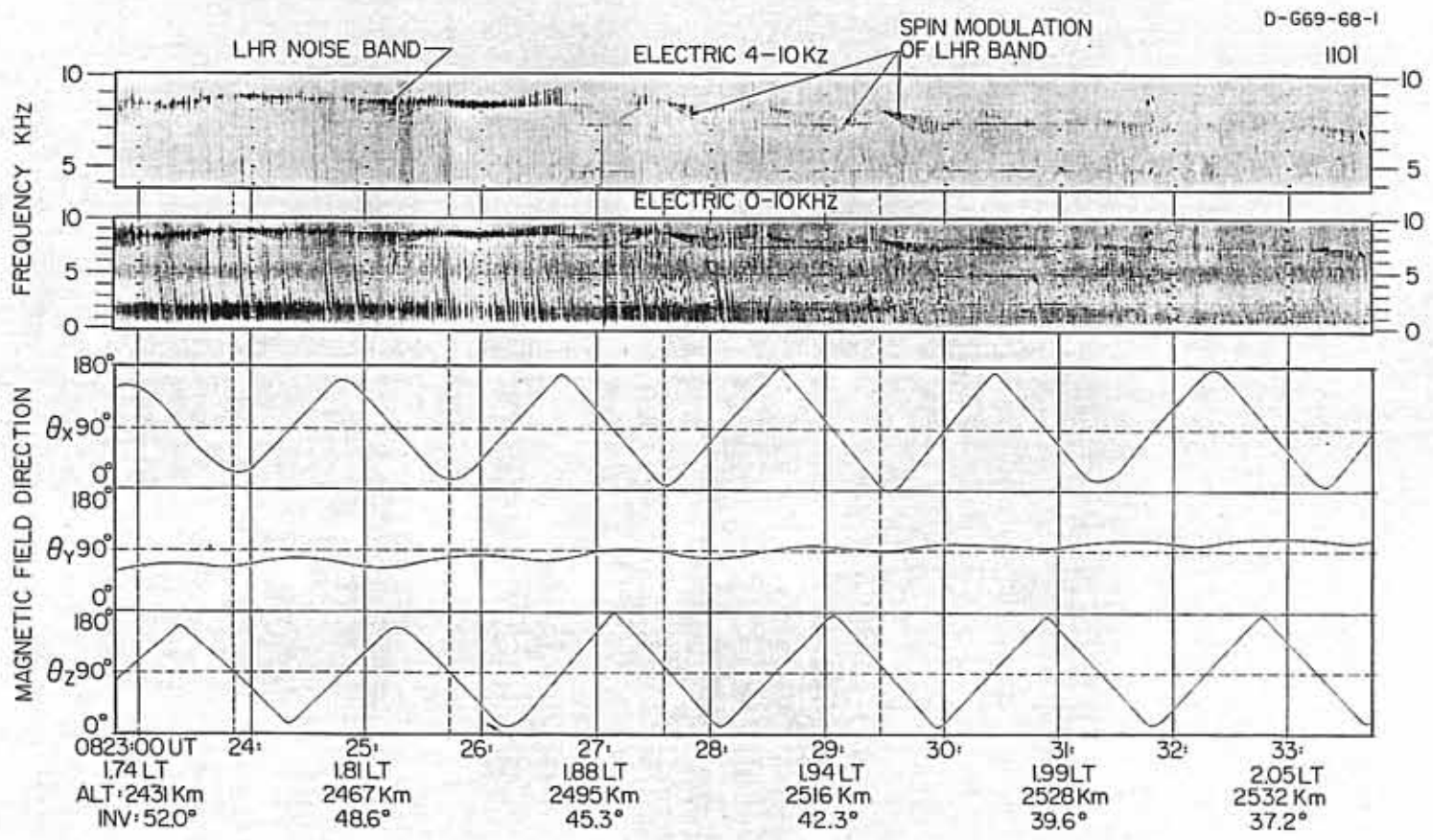
D-669-68-1
1101
LHR NOISE BAND
ELECTRIC 4-10Kz
SPIN MODULATION OF LHR BAND
ELECTRIC 0-10KHz
FREQUENCY KHz
10
5
0
MAGNETIC FIELD DIRECTION
180°
θx 90°
0°
θy 90°
θz 90°
0823:00 UT
1.74 LT
ALT: 2431 Km
INV: 52.0°
24:
25:
1.81 LT
2467 Km
48.6°
26:
27:
1.88 LT
2495 Km
45.3°
28:
29:
1.94 LT
2516 Km
42.3°
30:
31:
1.99 LT
2528 Km
39.6°
32:
33:
2.05 LT
2532 Km
37.2°

Figure 18. Spatial occurrence of spin modulation.

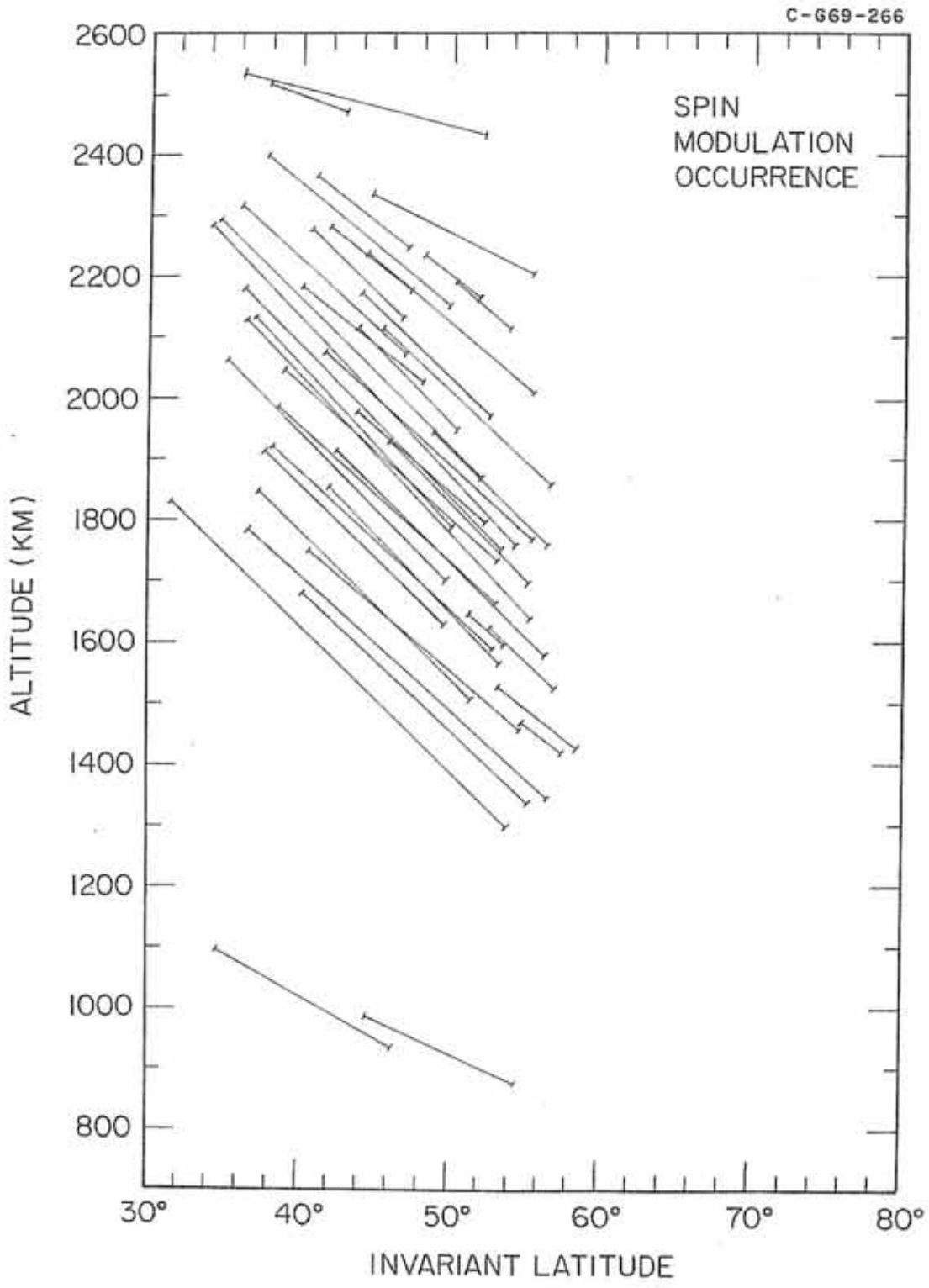
C-669-266
SPIN
MODULATION
OCCURRENCE
2600
2400
2200
2000
1800
1600
1400
1200
1000
800
ALTITUDE (KM)
30°
40°
50°
60°
70°
80°
INVARIANT LATITUDE

Figure 19. Typical electric receiver spectrograms from revolutions 53, 54, 115, 116, and 211.

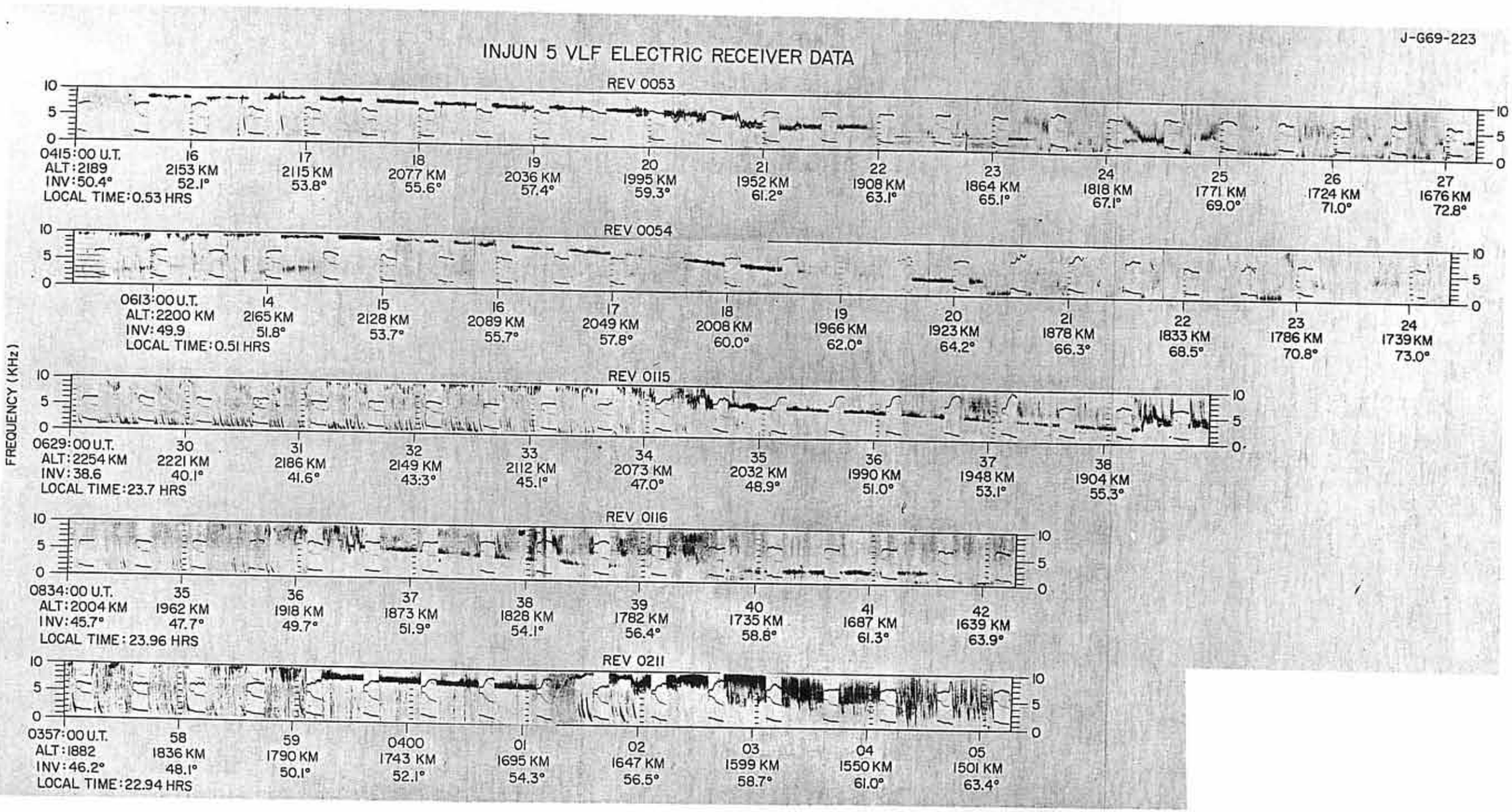
INJUN 5 VLF ELECTRIC RECEIVER DATA
J-G69-223
FREQUENCY (KHz)
REV 0053
0415:00 U.T.
ALT:2189
INV:50.4°
LOCAL TIME:0.53 HRS
16 2153 KM 52.1°
17 2115 KM 53.8°
18 2077 KM 55.6°
19 2036 KM 57.4°
20 1995 KM 59.3°
21 1952 KM 61.2°
22 1908 KM 63.1°
23 1864 KM 65.1°
24 1818 KM 67.1°
25 1771 KM 69.0°
26 1724 KM 71.0°
27 1676 KM 72.8°
REV 0054
0613:00 U.T.
ALT:2200 KM
INV:49.9
LOCAL TIME:0.51 HRS
14 2165 KM 51.8°
15 2128 KM 53.7°
16 2089 KM 55.7°
17 2049 KM 57.8°
18 2008 KM 60.0°
19 1966 KM 62.0°
20 1923 KM 64.2°
21 1878 KM 66.3°
22 1833 KM 68.5°
23 1786 KM 70.8°
24 1739 KM 73.0°
REV 0115
0629:00 U.T.
ALT:2254 KM
INV:38.6
LOCAL TIME:23.7 HRS
30 2221 KM 40.1°
31 2186 KM 41.6°
32 2149 KM 43:3°
33 2112 KM 45.1°
34 2073 KM 47.0°
35 2032 KM 48.9°
36 1990 KM 51.0°
37 1948 KM 53.1°
38 1904 KM 55.3°
REV 0116
0834:00 U.T.
ALT:2004 KM
INV:45.7°
LOCAL TIME:23.96 HRS
35 1962 KM 47.7°
36 1918 KM 49.7°
37 1873 KM 51.9°
38 1828 KM 54.1°
39 1782 KM 56.4°
40 1735 KM 58.8°
41 1687 KM 61.3°
42 1639 KM 63.9°
REV 0211
0357:00 U.T.
ALT:1882
INV:46.2°
LOCAL TIME:22.94 HRS
58 1836 KM 48.1°
59 1790 KM 50.1°
0400 1743 KM 52.1°
01 1695 KM 54.3°
02 1647 KM 56.5°
03 1599 KM 58.7°
04 1550 KM 61.0°
05 1501 KM 63.4°

Figure 20. Typical electric receiver spectrograms from revolutions 225, 272, 320, and 332.

E-G69-224

INJUN 5 VLF ELECTRIC RECEIVER DATA

REV 0225

0737:00 U.T.
ALT: 1718 KM
INV: 44.2°
LOCAL TIME: 22.92 HRS

38	39	40	41	42	43	44	45
1670 KM	1622 KM	1573 KM	1524 KM	1475 KM	1427 KM	1378 KM	1330 KM
46.4°	48.6°	51.0°	53.5°	56.1°	58.8°	61.6°	64.5°

REV 0272

0421:00 U.T.
ALT: 1574 KM
INV: 50.9°
LOCAL TIME: 22.48 HRS

22	23	24	25	26	27	28	29
1525 KM	1476 KM	1427 KM	1379 KM	1330 KM	1283 KM	1236 KM	1190 KM
53.3°	55.8°	58.4°	61.0°	63.7°	66.4°	69.1°	71.8°

FREQUENCY (KHz)

REV 0320

0302:00 U.T.
ALT: 1492 KM
INV: 49.3°
LOCAL TIME: 21.98 HRS

03	04	05	06	07	08	09	10
1443 KM	1395 KM	1346 KM	1299 KM	1251 KM	1205 KM	1160 KM	1116 KM
51.6°	54.0°	56.5°	59.0°	61.6°	64.2°	66.8°	69.5°

REV 0332

0240:00 U.T.
ALT: 1583 KM
INV: 44.0°
LOCAL TIME: 21.76 HRS

41	42	43	44	45	46	47	48
1533 KM	1484 KM	1435 KM	1387 KM	1338 KM	1291 KM	1244 KM	1197 KM
46.0°	48.2°	50.4	52.8°	55.2°	57.7°	60.3°	62.9°

Figure 21. Typical electric receiver spectrograms from revolutions 345, 370, 381, 382, and 749.

J-G69-225

INJUN 5 VLF ELECTRIC RECEIVER DATA

FREQUENCY (KHz)

REV 0345

0422:00 U.T.
ALT: 1394 KM
INV: 48.2°
LOCAL TIME: 21.78 HRS

23	24	25	26	27	28	29	30
1346 KM	1298 KM	1251 KM	1204 KM	1159 KM	1115 KM	1072 KM	1031 KM
50.9°	53.6°	56.4°	59.3°	62.3°	65.3°	68.3°	71.4°

REV 0370

0543:00 U.T.
ALT: 1250 KM
INV: 48.7°
LOCAL TIME: 21.63 HRS

44	45	46	47	48	49
1204 KM	1158 KM	1114 KM	1071 KM	1030 KM	990 KM
51.5°	54.4°	57.5°	60.6°	63.8°	67.1°

REV 0381

0317:00 U.T.
ALT: 1616 KM
INV: 35.2°
LOCAL TIME: 21.17 HRS

18	19	20	21	22	23	24	25	26	27
1567 KM	1517 KM	1468 KM	1419 KM	1370 KM	1322 KM	1274 KM	1227 KM	1181 KM	1137 KM
37.0°	38.9°	41.0°	43.3°	45.7°	48.2°	50.9°	53.7°	56.5°	59.4°

REV 0382

0519:00 U.T.
ALT: 1435 KM
INV: 38.0°
LOCAL TIME: 21.30 HRS

20	21	22	23	24	25	26	27	28	29
1386 KM	1337 KM	1289 KM	1242 KM	1196 KM	1157 KM	1151 KM	1064 KM	1023 KM	984 KM
40.2°	40.6°	45.2°	47.9°	50.7°	53.7°	56.7°	59.9°	63.1°	66.4°

REV 0749

0946:00 U.T.
ALT: 1258 KM
INV: 70.1°
LOCAL TIME: 4.57 HRS

47	48	49	50	51	52	53	54	55
1306 KM	1353 KM	1402 KM	1450 KM	1499 KM	1548 KM	1597 KM	1645 KM	1693 KM
67.5°	64.9°	62.4°	59.9°	57.5°	55.1°	52.9°	50.7°	48.6°